



## A kinetic model for SCR coated particulate filters—Effect of ammonia-soot interactions

Lidija V. Trandafilovic<sup>a</sup>, Oana Mihai<sup>a</sup>, Jungwon Woo<sup>a</sup>, Kirsten Leistner<sup>a</sup>, Marie Stenfeldt<sup>b</sup>, Louise Olsson<sup>a,\*</sup>

<sup>a</sup> Chemical Engineering, Competence Centre for Catalysis, Chalmers University of Technology, SE-412 96, Göteborg, Sweden

<sup>b</sup> Volvo Cars Corporation, SE-405 31, Göteborg, Sweden



### ARTICLE INFO

#### Keywords:

Soot  
DPF  
SCR coated filters  
Kinetic modelling  
Cu/SSZ-13

### ABSTRACT

SCR coated filters have recently been introduced. These combine soot capture through diesel particulate filters (DPF) and NO<sub>x</sub> removal through ammonia selective catalytic reduction (NH<sub>3</sub> SCR). This study investigates the impact of soot on the reactions being important for the SCR process on Cu/SSZ-13, as well as the impact of different gases on soot oxidation using flow reactor measurements. A limited impact of soot on the SCR reactions and a clear inhibiting effect of NH<sub>3</sub> on soot oxidation, is found. Ammonia TPD, *in-situ* DRIFT, and XPS experiments are used to investigate the interaction between soot and ammonia. Amines/amides are found on the soot when exposed to NH<sub>3</sub> and H<sub>2</sub>O. The results are used to develop a kinetic model for soot oxidation over DPF and a soot coated Cu/SSZ-13 catalyst using diesel soot generated from an engine bench. It is found that it is important to incorporate a random pore model and a free edge site mechanism through which ammonia blocks these free edge carbons. The model describes well soot oxidation in the presence of NH<sub>3</sub> over DPF, as well as soot oxidation and the SCR mechanism over soot loaded Cu/SSZ-13.

### 1. Introduction

It is critical to remove pollutants produced by engine exhausts such as unburned hydrocarbons, particulate matter (PM) and nitric oxides (NO<sub>x</sub>). Several different pollution control technologies have been developed so far. These include Diesel Particulate Filters (DPFs) (for the control of PM composed of soot and unburned carbonaceous compounds) [1], urea selective catalytic reduction (technology for the abatement of NO<sub>x</sub> [2–4]), and diesel oxidation catalysts (DOC) (for the control of hydrocarbon emissions and CO) [5]. The combination of selective catalytic reduction (SCR) and DPF, used in advanced after-treatment systems, is a great improvement, and there are pros and cons relating to the order in which SCR and DPF are placed. If the SCR-catalyst is placed upstream of the DPF, then the warm-up time for the SCR will be reduced and, cold start NO<sub>x</sub>-emissions will be reduced. However, less NO<sub>2</sub> reaches the DPF thus minimizing the potential for passive regeneration and increasing the frequency of active regeneration. If a DPF is placed in front of an SCR catalyst, this will be ideal from a regeneration point of view, but the DPF thermal mass results in a lower temperature in the SCR catalyst during the initial warm up of the system. At temperatures below 180–200 °C it is not possible to dose

urea because it will form deposits [6] and fast heat-up is therefore critical. In addition, there will be less available NO<sub>2</sub> for fast SCR, since it is used for soot oxidation. Integration of catalytic SCR and DPF technologies in an SCR coated filter is a promising technology [7,8], since the SCR functionalities quickly reach sufficient temperature, at the same time as the NO<sub>2</sub> is available for soot regeneration. It has been found that these systems also demonstrate high NO<sub>x</sub> conversion capabilities [9,10] together with soot removal.

Catalysts used in SCR coated filter systems are, e.g. vanadium based [7,11] or based on zeolites [8,12]. The copper ion-exchanged zeolites, e.g. Cu/SSZ-13, used for NH<sub>3</sub>-SCR have major advantages, such as high activity at low temperatures [13,14], high hydro-thermal stability [15], hydrocarbon resistance [16], and the ability to withstand prolonged operation at high temperatures [17,18]. The Cu/SSZ-13 has a chabazite (CHA) structure with small pores (3.8 × 3.8 Å) that are able to influence gas diffusion and give "shape selectivity" to gases such as NO<sub>x</sub>, N<sub>2</sub>O, and NH<sub>3</sub> (with dynamic diameters of 3.17, 3.83, and 2.90 Å, respectively) [19]. Moreover, it is suggested that the small pores are the reason for the high hydrothermal stability [20] and hydrocarbon resistance [16] of Cu/SSZ-13. Several kinetic models for NH<sub>3</sub>-SCR over Cu/zeolites have been developed that describe the mechanisms for NH<sub>3</sub>-SCR [21–24], sulfur poisoning [25], and hydrothermal

\* Corresponding author.

E-mail address: [louise.olsson@chalmers.se](mailto:louise.olsson@chalmers.se) (L. Olsson).

Nomenclature	
$A_i$	Pre-exponential factor for reaction i ( $s^{-1}$ )
$c_k^L$	Molar surface concentration of component k at washcoat layer ( $kmol/m^3$ )
$c_k^B$	Molar bulk concentration of component k ( $kmol/m^3$ )
$d_{hyd}$	Hydraulic diameter of the channel (m)
$d_{por}$	Pore diameter (m)
$D_{eff}$	Effective diffusivity ( $m^2/s$ )
$E_{A,i}$	Activation energy for reaction i (J/mol)
$GSA$	Geometric surface area per reactor volume ( $m^{-1}$ )
$h_k$	Total enthalpy of component k (J/mol)
$k_h$	Heat transfer coefficient between gas phase and solid walls ( $W/(m^2 K)$ )
$k_{k,m}$	Mass transfer coefficient of species k ( $mol/(m^2 s)$ )
$k_i$	Rate constant for reaction i ( $s^{-1}$ )
$L$	Length of channel (m)
$M_k$	Molar mass of gas phase species k (kg/kmol)
$p_g$	Partial pressure of gas
$r_i$	Reaction rate for reaction i ( $kmol/(s m^2)$ )
$R$	General gas constant (8.314 J/(mol K))
Re	Reynolds number
Sc	Schmidt number
Sh	Sherwood number
$T_s$	Temperature at catalyst surface (K)
$T_g$	Gas phase temperature (K)
$t$	Time (s)
$v_g$	Gas velocity (m/s)
$\nu_{i,k}$	Stoichiometric coefficient of species k in reaction i (-)
$w_{k,g}$	Mass fraction of species k in gas phase (-)
$w_{k,L}$	Mass fraction of species k in layer L (-)
$y_k$	Mole fraction at the reaction layer of specie k (-)
$y_k^B$	Mole fraction in the gas bulk of specie k (-)
$y$	Spatial coordinate in radial direction in washcoat layer (m)
$z$	Spatial coordinate in axial direction (m)
Greek letters	
$\varepsilon_g$	Porosity of gas phase in entire system (-)
$\varepsilon_{wcl}$	Porosity of the considered washcoat layer (-)
$\theta_k$	Coverage of species k (-)
$\psi$	Surface site density of storage site ( $mol/m^2$ )
$\Psi$	Initial pore structure factor (-)
$\lambda_g$	Thermal conductivity ( $W/(m K)$ )
$\rho_g$	Density of the gas phase ( $kmol/m^3$ )
$\rho_L$	Density of the gas mixture in the washcoat layer cell ( $kmol/m^3$ )
$\Delta H_i$	Heat of reaction i (kJ/mol)

deactivation [26].

Soot characteristics (chemical structure, reactivity, activation energies) are not easily summarised because they depend on engine type, on fuel composition (diesel, biodiesel, petrol) [27,28], fuel components [29–32], and driving conditions. The typical chemical composition of exhaust particulate matter is solid carbon covered with adsorbed hydrocarbons (HC) and a soluble organic fraction (SOF) [33,34]. The morphology of soot particles is complex as well, starting from primary small soot particles, with a size variation that depends on the fuel source, to growth by agglomeration, which forms chain-like aggregates essentially composed of spherical primary particles [35–37]. Several kinetic models have been developed to incorporate various complex aspects of soot: in multi-population model total soot mass is decomposed into several fractions, where every fraction has its own reaction rates [38] or a similar two-layer model where different soot activities are explained through interaction, or lack of it, with the catalyst [39]. A random pore model [40–42] and a shrinking core model [43–46], which is a special case of random pore model that takes into account the complexity of soot particles surface are also presented.

Experimental studies of an SCR coated filter show different results due to the complexity of soot combined with various catalyst properties in SCR coated filters. For instance, an increase in the ammonia amount adsorbed on the catalyst in the presence of PM has been observed, and, in some studies, a decrease in ammonia has been found [7,47]. Lee et al. [9] examined the effect of PM loading on NOx reduction in FTP tests and found that there was no influence on the  $NO_x$  reduction efficiency. However, Tang et al. [48] found that the PM loading improved the  $NO_x$  reduction in engine bench measurements and the reason for this is likely that they used a high  $NO_2/NO_x$  ratio (ca 68%). Since the  $NO_2/NO_x$  level was above 50% it is beneficial to reduce it for fast SCR conditions (50%) and this can be done by oxidation of the soot. In addition, earlier work [49] have found that the presence of soot decreases the inhibition effect of ammonium nitrates at low temperatures in fast SCR conditions. Tronconi et al. [50] found that the passive PM oxidation rate is influenced by SCR reactions since  $NO_2$  is consumed by the fast SCR reaction. SCR coated filters have also been found to have good thermal durability and high robustness [48,51,52].

Some simulation models in which soot oxidation and SCR reactions

are modelled simultaneously are developed to better understand SCR coated filters [53–57]. For example, Watling et al. [57] have developed a kinetic model for an SCR coated filter that combines an SCR kinetic model of a flow-through monolith and a model of a coated DPF, with the assumption that the catalyst does not affect soot oxidation kinetics. Colombo et al. [56], have used an existing SCR kinetic model for a catalysed DPF to assess the impact of soot. Those authors, concluded that a competition between soot oxidation and deNOx processes involving  $NO_2$  occurs.

Although there is documented negative influence of  $NH_3$  on soot oxidation [58,59], to the best of our knowledge, there are no kinetic models that include the interaction of  $NH_3$  and soot during soot oxidation. The aim of the present work, therefore, is to develop a kinetic model for DPF and SCR-filters using diesel soot generated from an engine bench. First, we developed a model for soot oxidation,  $NH_3$  oxidation, and  $NH_3$ -SCR on DPF. Thereafter the developed model was used and tested on a Cu/SSZ-13 catalyst impregnated with soot. It was found that the developed kinetic model describes well the DPF as well as the different reactions on the Cu/SSZ-13 catalyst impregnated with soot.

## 2. Experimental

### 2.1. Catalyst preparation

In the first step, zeolite Na/SSZ-13 was synthesized according to the following procedure: A solution of sodium silicate (320 g of milliQ water and 250 g of sodium silicate (SigmaAldrich 338443-1 L)) was added to a 200 ml solution of 1 M NaOH (SigmaAldrich, > 98% anhydrous pellets), and the mixture was stirred for 15 min. Afterwards Zeolite Y (CBV712 from Zeolyst International) was added to the solution, and the mixture was stirred for an additional 30 min. Finally, 105 g of a TMAAI solution (25% solution of tricyclo[3.3.1.13,7]decane-1-aminium,*N,N,N*-trimethyl-,hydroxide from Sachem, ZeoGen SDA 2825) was added, and the system was stirred for another 30 min. The prepared mixture was transferred to a Teflon lined autoclave and heated to 140 °C for six days (including the time to heat up from room temperature). After six days, the autoclave was cooled to room temperature, and the liquid was decanted. The solid was repeatedly washed

with milliQ and centrifuged until pH was neutral. Afterwards it was dried at room temperature. The obtained powder was calcined for 8 h at 550 °C (with a ramp of 0.5 °C/min).

In the second step, which was performed twice, an ammonium form of Na/SSZ-13 was synthesized by treating Na/SSZ-13 with 0.25 M NH<sub>4</sub>NO<sub>3</sub>. The ratio of the volume of solution (mL) of NH<sub>4</sub>NO<sub>3</sub> to the weight of zeolite Na/SSZ-13 (g) was 1000:30. First the Na/SSZ-13 powder was slowly added to the NH<sub>4</sub>NO<sub>3</sub> solution, and the system was then continuously stirred and kept at 80 °C for 15 h. After the ion exchange, the sample was cooled to room temperature and the liquid was removed. The powder was then washed and centrifuged seven times with milliQ water. A Cu exchange was done in the third step, which was repeated three times. 273 ml milliQ water solution of 0.2 M Cu(NO<sub>3</sub>)<sub>2</sub> was heated to 80 °C at which point the zeolite from the previous step was added. After 120 min of stirring at 80 °C, the system was left to cool to room temperature, and the liquid was removed. The resulting powder was washed with milliQ water until a neutral pH was achieved. Finally, the powder was dried for 12 h at room temperature and calcined in air at 550 °C for 4 h (time for heating and cooling is not included in the 4 h). The heating and cooling were done at a ramping rate of 5 °C/min to the set temperature.

The Cu/SSZ-13 powder was washcoated on a 400 cpsi monolith, with the dimensions 2 cm in length and 2.1 cm in diameter. In order to improve the adhesion of the zeolite layer, a thin alumina layer was first applied (75 mg) to the monolith and was followed by a zeolite coating (750 mg) using 5% of a boehmite binder. The prepared monolith was calcined in an oven at 500 °C for 2 h (time for heating and cooling is not included in the 2 h), using a heating and cooling rate of 5 °C/min ramp.

## 2.2. Catalyst characterization

The Brunauer-Emmett-Teller (BET) surface area and pore volume of the Cu/SZZ-13 were measured using N<sub>2</sub> physisorption at -195 °C with a Micromeritics ASAP 2010 instrument after the powder had been degassed at 240 °C for 3 h under vacuum. An elemental analysis was performed using an inductively coupled plasma sector field mass spectrometer (ICP-SFMS) by ALS Scandinavia AB. The crystalline structure of the synthesized catalyst was then characterized using a Bruker AXS XRD.

## 2.3. Soot characterization

The interaction of ammonia and water with the soot was studied with *in situ* diffuse reflectance infrared Fourier transform spectroscopy (DRIFTS) experiments. This was done using a Bruker Vertex 70, and each spectrum was recorded at 4 cm<sup>-1</sup> resolution. After loading the soot sample mixed with KBr at the ratio 70:30, it was cleaned at 500 °C in flowing argon (200 mL/min) for 20 min. After cleaning, the sample was cooled to the desired reaction temperature (100 °C) under flowing argon. Before introducing the reactive gases, the starting spectrum was taken as a reference point. Thereafter the sample was exposed to a gas mixture of 1000 ppm NH<sub>3</sub> in Ar in the presence of 1% H<sub>2</sub>O for 1 h, during which DRIFT spectra were recorded.

X-ray photoelectron spectroscopy (XPS) measurements were done on a Perkin Elmer PHI 5000C ESCA system equipped with a monochromatic Al K X-ray source with an energy of 1486.6 eV. Two soot samples were measured: one sample without pretreatment and one sample that was treated with H<sub>2</sub>O and NH<sub>3</sub>. The untreated soot sample was directly measured with XPS without any pretreatment. The soot samples treated with water and ammonia were first loaded in a DRIFT cell and cleaned with Ar (200 mL/min) for 20 min at 500 °C. After this, the sample was cooled to 100 °C and treated with 1% H<sub>2</sub>O and 1000 ppm of NH<sub>3</sub> for 30 min. Afterward the sample was removed from the DRIFT cell and immediately transferred to the XPS chamber. Measurement started as soon as the XPS chamber reached sufficient low pressure.

A FEI Quanta 200 ESEM using a field emission gun equipped with an Oxford Inca energy dispersive X-ray (EDX) instrument was used to collect the images of the samples in low-vacuum mode (LV).

The density of the soot was measured using tap method. In short tapped bulk density is achieved by mechanically tapping a measuring cylinder containing the soot. After observing the initial volume, the cylinder is tapped until no volume change is observed (15 min). The measured density of the soot was 250 kg/m<sup>3</sup>.

## 2.4. Soot washcoating

Soot was loaded on a commercial DPF using the engine bench at Volvo Cars [59]. The preparation of the DPF for the soot oxidation experiment is explained in detail elsewhere [59]. Briefly, the DPF was soot loaded in an engine bench and thereafter cut into 7 slices. We used one of the middle slices to cut small cores from that were used in the experiments.

Soot was removed from the filter and dissolved in ethanol. Monolith cores, which were either empty or previously washcoated with Cu/SSZ-13, were impregnated with the soot and ethanol solution. The monolith samples were then heated in an oven (280 °C for 15 min) until the ethanol was removed. Before the experiments, the monolith samples were heated in Ar at 500 °C for 30 min to remove any possible stored hydro carbons. A SEM image from scraped off soot is shown in Fig. S1a (Supplementary material) and irregular soot particles of different size is observed. Moreover, in Fig. S1b a measurement of soot treated with ethanol is presented and no clear differences are observed between before and after ethanol treatment, indicating that ethanol do not impact soot.

The volume of the soot mass was calculated from the mass and diesel soot density for soot washcoating thickness, and it was assumed that this volume of soot was evenly distributed throughout the monolith channels. The soot washcoat thickness was measured by SEM of monolith channels with only washcoated soot, as presented in Fig. S2a-b (Supplementary material). For the soot wash-coating of the SCR catalyst, 70 mg of soot was loaded, and the thickness of the soot layer was estimated to be 16 µm, and this value was in agreement with SEM measurements where the washcoat thickness was in the range from 10 till 18 µm.

It should be noted that, for the ramping experiments, cores with soot were cut from the DPF and used directly in the flow reactor. The soot loading in the DPF was about 16.6 g/l (intentionally high loading to observe clear effects), which gave about 90 mg soot per sample and this results in an average soot thickness of 22 µm. Since the soot is primarily only on every second channel due to the plugged channels in the soot loading, we use a wash-coat thickness of 44 µm for the channels with soot. In the simulations we simulate one channel with soot and calculates the concentration out from the monolith by averaging over one channel with soot and one without (gives no CO and CO<sub>2</sub>). We also conducted simulations with an average 22 µm wash-coat for all channels and only minor differences were observed.

## 2.5. Flow reactor experiments

A flow reactor was used to determine the activity and selectivity of the samples, with and without the presence of soot, and the setup is described elsewhere [60]. Briefly, the reactor consisted of several massflow controllers and a CEM (Control - Evaporation - Mixing) system (Bronkhorst) for water delivery with vapor control. The mixed gas enters the quartz reactor where the monolith is placed. The temperature is measured inside and before the monolith. The activity for standard SCR, NH<sub>3</sub> oxidation, NH<sub>3</sub> temperature programmed desorption (TPD), and soot oxidation was measured, and the resulting gases (NH<sub>3</sub>, NO, NO<sub>2</sub>, N<sub>2</sub>O, CO, CO<sub>2</sub> and H<sub>2</sub>O) were detected with an MKS Multigas 2030 FTIR spectrometer.

Soot oxidation in the DPF experiments was carried out in a gas flow

of 3000 ml/min under atmospheric pressure. The sample pretreatment was done in Ar at 500 °C for 20 min before the experiments to remove the adsorbed hydrocarbons. After cooling to 200 °C, the samples were exposed to various gas feeds, and, thereafter, the temperature was increased to 750 °C at a rate of 2 °C/min. The gas concentrations in the experiments were as follows: soot oxidation was done in 8% O<sub>2</sub> and 5% H<sub>2</sub>O; for the NH<sub>3</sub> oxidation experiment, a mixture of 400 ppm NH<sub>3</sub>, 8% O<sub>2</sub>, and 5% H<sub>2</sub>O was used; and for the NH<sub>3</sub>-SCR 400 ppm NO, 400 ppm NH<sub>3</sub>, 8% O<sub>2</sub>, and 5% H<sub>2</sub>O was used. All these experiments were conducted on flow-through monoliths cut directly from the soot loaded DPF. More information relating to these experiments can be found in [59].

For the SCR filter experiments, a total flow of 2900 ml/min was used with argon as the inert balance in all experimental sequences. The catalyst (experiment without soot) was initially degreened using 400 ppm NO, 400 ppm NH<sub>3</sub>, 8% O<sub>2</sub>, and 5% H<sub>2</sub>O for 2 h at 700 °C. Thereafter, the catalyst was pretreated to clean the surface by exposing it to 8% O<sub>2</sub> and 5% H<sub>2</sub>O at 700 °C for 20 min. This pre-treatment was conducted prior to all experiments to achieve a clean surface when starting each experiment. The experimental conditions for the standard SCR experiment were 400 ppm of NH<sub>3</sub>, 400 ppm of NO, 8% O<sub>2</sub>, and 5% H<sub>2</sub>O, balanced with argon, and the temperature was increased stepwise, with a rate of 20 °C/min from 100 °C to 600 °C (700 °C in experiments with soot).

In the case of NH<sub>3</sub> oxidation, the catalyst was exposed to 400 ppm of NH<sub>3</sub>, 8% O<sub>2</sub>, and 5% H<sub>2</sub>O with a temperature increase same as for the NH<sub>3</sub>-SCR experiments. An ammonia temperature programmed desorption (NH<sub>3</sub> TPD) experiment was conducted with an adsorption phase at 100 °C for 3 h in the presence of 400 ppm NH<sub>3</sub> and 5% H<sub>2</sub>O. This was followed by flushing the catalyst for 90 min using 5% H<sub>2</sub>O in Ar and thereafter conducting a temperature ramp to 600 °C (700 °C when soot was present) at a ramp speed of 10 °C/min while the catalyst was exposed to 5% H<sub>2</sub>O in Ar. After the experiments (NH<sub>3</sub> SCR, NH<sub>3</sub> oxidation, NH<sub>3</sub> TPD) without soot, all the monoliths that were used were loaded with 10 g of soot per liter of monolith volume. Before repeating the experiments, monoliths were cleaned at 500 °C with 5% H<sub>2</sub>O in Ar for 30 min. All the experiments (NH<sub>3</sub>-SCR, NH<sub>3</sub> oxidation, NH<sub>3</sub> TPD) were repeated with soot present, with the same gas concentration, and in the same conditions except that the maximum temperature was set to 700 °C for all experiments.

In addition, soot oxidation experiments in the presence of O<sub>2</sub> and H<sub>2</sub>O were conducted on a Cu/SSZ-13 monolith impregnated with soot. First the sample was pretreated at 500 °C in the presence of 5% H<sub>2</sub>O in Ar for 30 min. After this, the sample was cooled to 100 °C, and the soot oxidation experiment in the presence of 5% H<sub>2</sub>O and 8% O<sub>2</sub> in Ar was started. The temperature for this experiment was increased at interval of 50 °C or 100 °C until 700 °C was reached.

### 3. Reactor model

Kinetic modelling was performed with a commercial software, AVL BOOST, version 2013 [61], using a one dimension (1D) single channel model. The channel was discretized in the axial direction using 20 grid points, with a grid shape factor set to 1. For the DPF simulations, only one layer in the washcoat layer (WCL) model (AVL Boost) was used. For the simulation of SCR filters, the WCL model had two layers, catalyst and soot, with specific transport and reaction model for each washcoat layer respectively. The model accounts for both mass transfer and heat transfer in gas bulk and wash-coat, which will be described in following paragraphs. In all simulations of ramping experiments, a linear inlet temperature was used. There was only a small temperature increase observed in the experiment and the reason for this was that we intentionally used a low heating rate (2 °C/min) in the ramp. The model well describes the produced heat in these experiments, see Supplementary material for details.

The species conservation equation used is [61]:

$$\varepsilon_g \frac{\partial \rho_g w_{k,g}}{\partial t} = -\varepsilon_g \frac{\partial \rho_g w_{k,g} v_g}{\partial t} + \varepsilon_g \frac{\partial}{\partial z} \left( \rho_g D_{eff} \frac{\partial w_{k,g}}{\partial z} \right) + M_k \sum_i^I v_{i,k} \dot{r}(c_k^L, T_s) \quad (1)$$

For definitions of used symbols, see nomenclature list. The coverage of different surface species  $\theta_k$  is determined by the following equation [61]

$$\frac{\partial \theta_k}{\partial t} (\Theta \cdot GSA) = \dot{r}_k \quad k = 1 \dots K \quad (2)$$

where the physical interpretation of the product ( $\Theta \cdot GSA$ ) is the entire storage capacity and it is based on the site density ( $\Theta$ ) and the geometrical surface area (GSA). The GSA is calculated by

$$\frac{GSA}{d_{hyd}} = 4 \times (\text{cell density}) \quad (3)$$

The energy balance for the gas phase is [61]

$$\begin{aligned} \varepsilon_g \frac{\partial}{\partial t} \left( \rho_g \sum_k^K w_{k,g} h_k \right) &= -\varepsilon_g \frac{\partial}{\partial z} \left( \rho_g \sum_k^K w_{k,g} h_k v_g \right) + \varepsilon_g \frac{\partial}{\partial z} \left( \lambda_g \frac{\partial T_g}{\partial z} \right) \\ &\quad + \varepsilon_g \frac{\partial}{\partial z} \left( \rho_g D_{eff} \frac{\partial w_{k,g}}{\partial z} h_k \right) + GSA \cdot k_h (T_s - T_g) \\ &\quad - \sum_i^I \Delta H_i \dot{r}(c_k^L, T_s) \end{aligned} \quad (4)$$

and for the solid phase [61]

$$(1 - \varepsilon_g) \rho_s \frac{\partial c_{p,s} T_s}{\partial t} = (1 - \varepsilon_g) \frac{\partial}{\partial z} \left( \lambda_s \frac{\partial T_s}{\partial z} \right) - GSA \cdot k_h (T_s - T_g) + \sum_i^I \Delta H_i \dot{r}(c_k^L, T_s) \quad (5)$$

The mass transfer from the gas bulk to catalyst surface is described by the film model according to [61]

$$GSA \cdot k_{k,m} (c_k^L - c_{p,g}^B) = \sum_i^I \dot{r}_i(c_k^L, T_s) \quad (6)$$

The Hawthorn correlation was used for calculating the Sherwood and Nusselt number [62] which is used to retrieve the mass and heat transfer coefficients,  $k_{k,m}$  and  $k_h$ , respectively:

$$Sh = 3.66 (1 + 0.095 Re Sc \frac{d_{hyd}}{L})^{0.45} \quad (7)$$

$$Nu = 3.66 (1 + 0.095 Re Sc \frac{d_{hyd}}{L})^{0.45} \quad (8)$$

The mass transfer in the washcoat was simulated using 5 grid points and the balance equation for specie k, solved for each cell, is [61]:

$$\varepsilon_{wcl} \frac{\partial \rho_L w_{k,L}}{\partial y} = \frac{\partial}{\partial y} \left( \rho_L D_{k,eff} \frac{\partial w_{k,L}}{\partial y} \right) + M_k \sum_i^I v_{i,k} \bar{r}_i(c_k^L, T_s) \quad (9)$$

The effective diffusivity of the different gas components were calculated using random pore diffusion model developed by Wakao and Smith [63] and the used equations are given in the Supplementary material. It should be noted that also effective pore diffusion and parallel pore diffusion models were used and same results were retrieved. We have intentionally used thin washcoats in order to minimize mass-transfer simulations.

We estimated the washcoat thickness of Cu/SSZ-13 zeolite using the results of Metkar et al. [64] according to which a washcoating loading of 0.15 g/cm<sup>3</sup> gives an average washcoat thickness of about 35 µm. Our estimation gave that, in case of a monolith with 20 mm length and 21 mm diameter and catalyst mass of 750 mg, the washcoat thickness would be approximately 25 µm. This value was confirmed in SEM measurements of washcoated monolith where washcoat thickness was in the range from 22 to 27 µm as presented in Fig. S2c-d) (Supplementary material). The thickness of the soot layer in the model is

described in Section 2.4 relating to soot loading.

The Arrhenius equation was used for determining the rate constants as

$$k_i = A_i \times \exp(-E_{A,i}/RT_s) \quad (10)$$

## 4. Result and discussion

### 4.1. Catalyst characterization

The XRD measurements (results presented in Supplementary material, Fig. S4) of the powder zeolite sample confirmed the structure of the SSZ-13. The zeolite structure remained intact after the ion-exchange to form Cu/SSZ-13. ICP-SFMS was used for elemental analysis, and it was found that the SiO<sub>2</sub> to Al<sub>2</sub>O<sub>3</sub> ratio was 11, and the Cu loading level was 4.5 wt.%. This resulted in an exchange level of 0.31 Cu/Al. Further, sodium and iron were below the detection level of the ICP (< 0.04 wt.% and < 0.06 wt.%, respectively). The BET surface area of Cu/SSZ-13 was 555.3 m<sup>2</sup>/g.

### 4.2. Effect of gas composition on soot oxidation

The influence of soot on Cu/SSZ-13 activity was studied in three main experiments: NH<sub>3</sub>-SCR, NH<sub>3</sub> oxidation, and soot oxidation in the presence of O<sub>2</sub> and H<sub>2</sub>O. In these experiments, the catalyst was first impregnated with soot (see detailed information in the experimental section), followed by pre-treatment in Ar at 500 °C. Thereafter the sample was exposed to the reaction mixture starting at 100 °C and increasing the temperature in increments of 50 °C or 100 °C, which allowed the CO and CO<sub>2</sub> caused by soot oxidation to be monitored for each step. The amount of oxidized soot was derived from this data and is presented as a function of the temperature step in Fig. 1. Note that the soot oxidized during the heating between the steps was added to the subsequent temperature step. On the basis of these measurements, the total soot loading for our experiments was roughly 10 g/L. This assumes that all soot was oxidized at 700 °C, which is in line with finding in the literature [65,66].

Fig. 1 shows that, adding 400 ppm NH<sub>3</sub> had a negative influence on soot oxidation and shifted combustion toward a higher temperature, which is in line with our previous study [59]. The activity for soot oxidation was regained in NH<sub>3</sub>-SCR conditions. At this temperature, the SCR zone was very short [67], and NH<sub>3</sub> was quickly removed in the SCR reaction. The majority of the catalyst was therefore, not exposed to NH<sub>3</sub>.

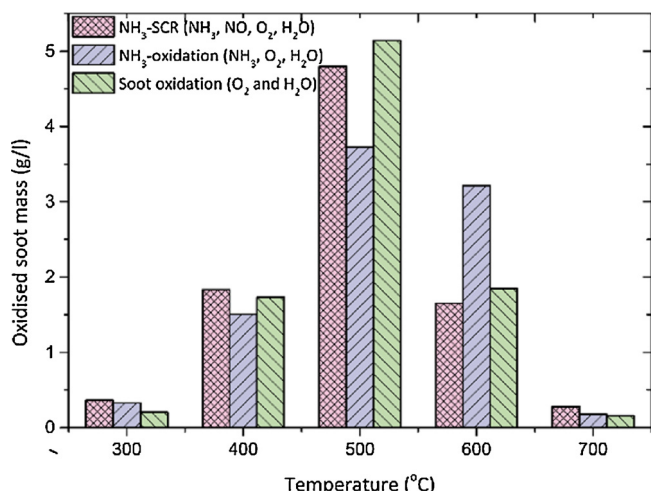


**Fig. 1.** Soot mass calculated from CO and CO<sub>2</sub> produced during experiments in which the temperature was increased stepwise in different gas mixtures (NH<sub>3</sub>-SCR, NH<sub>3</sub> oxidation and oxidation) over soot loaded Cu/SSZ-13.

### 4.3. Interaction between H<sub>2</sub>O, NH<sub>3</sub> and soot

The effect of soot on NH<sub>3</sub> storage was examined in the NH<sub>3</sub>-TPD experiment. The resulting ammonia desorption, with and without soot, versus catalyst temperature is presented in Fig. 2. In these experiments, the catalyst (with and without soot) was exposed to 400 ppm NH<sub>3</sub> and 5% H<sub>2</sub>O at 100 °C. The estimated ratio of mass NH<sub>3</sub> per soot mass is about 2.5, thus the sample was exposed to large amount of ammonia. This was followed by a period of 5% H<sub>2</sub>O in argon after which the temperature was increased to 600 °C (the experiment without soot) and to 700 °C when soot was present (Supplementary Fig. S5). When NH<sub>3</sub> in the inlet gas was shut off, loosely bound ammonia started to desorb at 100 °C, and when the temperature was increased, stronger bound NH<sub>3</sub> desorption was visible. The initial desorption at 100 °C corresponded to the physisorbed ammonia. Beside the dominant peak, located at 335 °C, a shoulder was also detected at 459 °C. The middle and high temperature peaks are associated with ammonia storage in different copper and Bronsted acid sites [21]. A deconvolution using three peaks was conducted and is shown in Fig. 2b, which shows a very good fit. The existence of multiple storage sites in a Cu/SSZ-13 structure was experimentally confirmed in earlier studies [21,68–71]. Three different ammonium storage sites were in line with the kinetic model for NH<sub>3</sub> storage over Cu/SSZ-13 proposed by Olsson et al. [21].

The comparison between NH<sub>3</sub>-TPD with and without soot showed that slightly more NH<sub>3</sub> was desorbed at a high temperature with soot, which is in agreement with our earlier study using a supplier SCR coated filter [49]. These results indicate that some ammonia adsorbed on the soot particles, and the binding strength was strong since the additional ammonia desorbed at a higher temperature. However, the difference between the desorption profiles are small and can be within the experimental error.

To further study the interactions between soot and ammonia, an *in-situ* DRIFT experiment was performed. Fig. 3 shows the DRIFT results for the soot sample exposed to Ar only at 100 °C just after the background is taken, thus before introducing the reactive gases (black line). This was done in order to more clearly observe the results when adding NH<sub>3</sub>+H<sub>2</sub>O, which is shown by the green line in Fig. 3. Three strong bands were detected in the spectrum. The stretching vibrations of the hydroxyl groups, caused by the presence of water, were detected in the region above 3500 cm<sup>-1</sup> [72,73]. Absorption bands of gaseous CO<sub>2</sub> occurred at 2420–2305 cm<sup>-1</sup> because of the surface oxidation of a small amount of soot. Gaseous NH<sub>3</sub> in combination with water vapor absorption bands were detected in the 1300–2000 cm<sup>-1</sup> region [74,75]. Interestingly, the band at 1000–1140 cm<sup>-1</sup> and, the band at 1240 cm<sup>-1</sup> were due to the formation of amines and/or amide (-C-NH<sub>2</sub>) groups [76–79]. To conclude, the bands at 1240–1000 cm<sup>-1</sup> in the figure clearly show that there was an interaction between soot and NH<sub>3</sub> and that it occurred in the form of amines and/or amides, but that there is still significant amount of hydroxyl groups present.

The interaction between NH<sub>3</sub> and water with soot was also studied with XPS. Fig. 4 shows a survey scan together with high-resolution scans over the C1s, O1s, and N1s regions for diesel soot produced from the engine bench at Volvo Cars, without and with NH<sub>3</sub> and H<sub>2</sub>O treatment. The survey scans, presented in Fig. 4a, for all soot samples show the existence of C1s and O1s peaks. The deconvolution of the high resolution C1s peak (green dots) for the original soot sample shows multiple peaks positioned at 284.5, 285.4, 286.6, and 288.4 eV. The cumulative fit is presented as a red line in Fig. 4b. Identification was as follows: 284.5 eV corresponded to the C-C sp<sup>2</sup> and 285.4 eV was interpreted as a C-C sp<sup>3</sup> hybridized carbon [29]. Additional peaks were identified as phenolic elements of soot (C-OH) at 286.6 eV and a carbonyl (C=O) group at 288.4 eV [28,31,32,80]. The sp<sup>2</sup> content was interpreted as graphitic carbon, and the sp<sup>3</sup> was interpreted as aliphatic carbon [28,80]. The dominant graphitic carbon contribution to the C1s peak together with the peak from oxidized carbon, in diesel soot, was also detected by Uy et al. [28]. The results of soot treated with H<sub>2</sub>O and

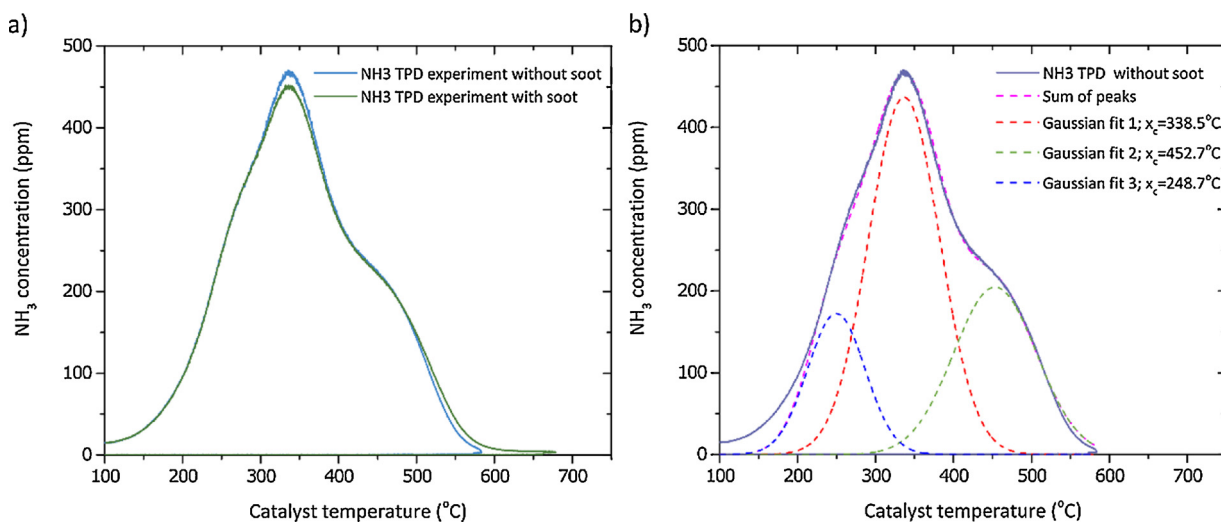


**Fig. 2.** NH<sub>3</sub>-TPD experiment with and without impregnated soot over a Cu/SSZ-13 monolith.

NH<sub>3</sub> plus H<sub>2</sub>O are also presented (Fig. 4b) and show a similar C1s peak shape.

The O1s high resolution scans of soot (green dots), soot after exposure to H<sub>2</sub>O (black dashed line), and soot after exposure to H<sub>2</sub>O plus NH<sub>3</sub> (blue dotted line) are presented in Fig. 4c. The O1s spectrum exhibits a peak at 531.4 eV, which could be assigned either to a C—O—C or a C=O bond. The peak at 533.5 eV refers to the carbon-oxygen single bond in hydroxyl groups (C—O—H) [81–83]. The broad peak at 535.9 eV can be assigned to physisorbed O<sub>2</sub> [84], chemisorbed water, or differential charging [81,82]. However treating a soot sample with water vapor reduced the contribution of the 535.9 eV peak and increased contribution of 533.5 eV (C—O—H). Therefore, it was concluded that the peak at 535.9 eV was likely associated with physisorbed O<sub>2</sub>. The addition of ammonia had the opposite effect on reducing the contribution of the 533.5 eV peak within the O1s spectrum.

Fig. 4d shows that NH<sub>3</sub> groups on the surface of the soot were detected after exposure of soot to NH<sub>3</sub> and H<sub>2</sub>O, although in small amount. Binding energy at 400 eV was identified as NH<sub>2</sub> groups [85], while the adsorbed NH<sub>3</sub> was detected at 402 eV [86]. Our *in-situ* DRIFT and XPS experiments showed surface OH groups and amines or amides on the soot surface during and after exposure to ammonia and H<sub>2</sub>O vapour, and this was the base for our kinetic model development.

#### 4.4. Kinetic models for diesel particulate filter (DPF)

##### 4.4.1. Kinetic model for soot oxidation in the presence of O<sub>2</sub> and H<sub>2</sub>O

Soot oxidation in the presence of 8% O<sub>2</sub> and 5% H<sub>2</sub>O was studied with a temperature ramp from room temperature to 700 °C using cores cut from a DPF loaded with soot in engine bench [59]. A plot of ln(k) as a function of 1/T, using Arrhenius equation Eq.(10), gives the activation energies for CO<sub>2</sub> and CO production [45], as presented in Fig. 5. As can be seen from the slope in the figure, there are two regions for the activation energies, depending on the temperature range. Below 494 °C, the activation energy was 77.2 kJ/mol for CO<sub>2</sub>, and for temperature above 494 °C, it was 140.6 kJ/mol. The corresponding values for CO formation was 87.5 and 123.4 kJ/mol (see Fig. 5b). As can be seen in Fig. 6, the temperature range for the main soot oxidation was above 500 °C, therefore, the second activation energy was used in simulations (140.6 kJ/mol and 123.4 kJ/mol). The chosen value was very close to the already documented value of 142 kJ/mol [87,88] and 148 kJ/mol [89], and within the range of the values mentioned by various authors [45,90,91].

A simple model for soot oxidation to CO<sub>2</sub> and CO was examined using Equations R.1 and R.2 in Table 1. The  $\psi_C$  represents surface site density and the  $\theta_C$  represents the loading ratio between carbon at some

point in time compared to the initial loading of carbons. The surface site density of soot,  $\psi_C$ , was determined so that the integrated sum of CO and CO<sub>2</sub> was the same in simulation and experiment, thus having same surface density of soot. Heat of reactions for soot oxidation to form CO and CO<sub>2</sub> of –99 kJ/mol and –393 kJ/mol, respectively, was used. The results of the simulation (red dashed line) using Equations R.1 and R.2 with experimental data (green and blue lines) are presented in Fig. 6. The activation energies used are from the Arrhenius plot (see Fig. 5), and the pre-exponential factors were manually tuned. These simple reaction rates cannot describe the experimental features. This is likely due to the linear dependence of soot sites, which is not the case for highly porous carbon, like soot or activated carbon, where the specific surface area can increase as a function of conversion due to the existence of porosity [92]. This leads to the conclusion that a complex soot structure and changes in soot reactivity and morphology during oxidation [93,94] must be included in the soot oxidation kinetic model.

Soot complexity is evident even from the point of particle size. Soot from a diesel engine has particles in three main size ranges. According to Twigg et al. [95], these are 5–20 nm (nanoparticles in the nuclei mode), 30–1000 nm (ultrafine particles in the accumulation mode), and 1–20 μm (the coarse mode). Even the composition of soot greatly varies, depending on the source [96,97]. The shape and size of our soot

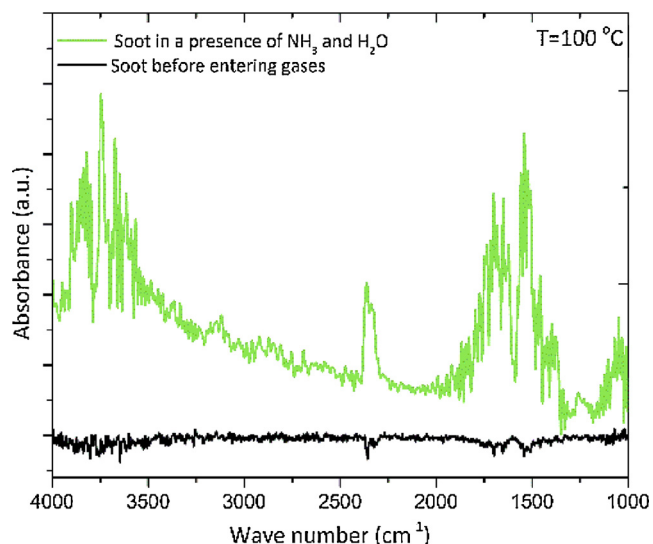


**Fig. 3.** DRIFT result of soot in the presence of NH<sub>3</sub> and H<sub>2</sub>O at 100 °C compared to soot spectrum after background with Ar.

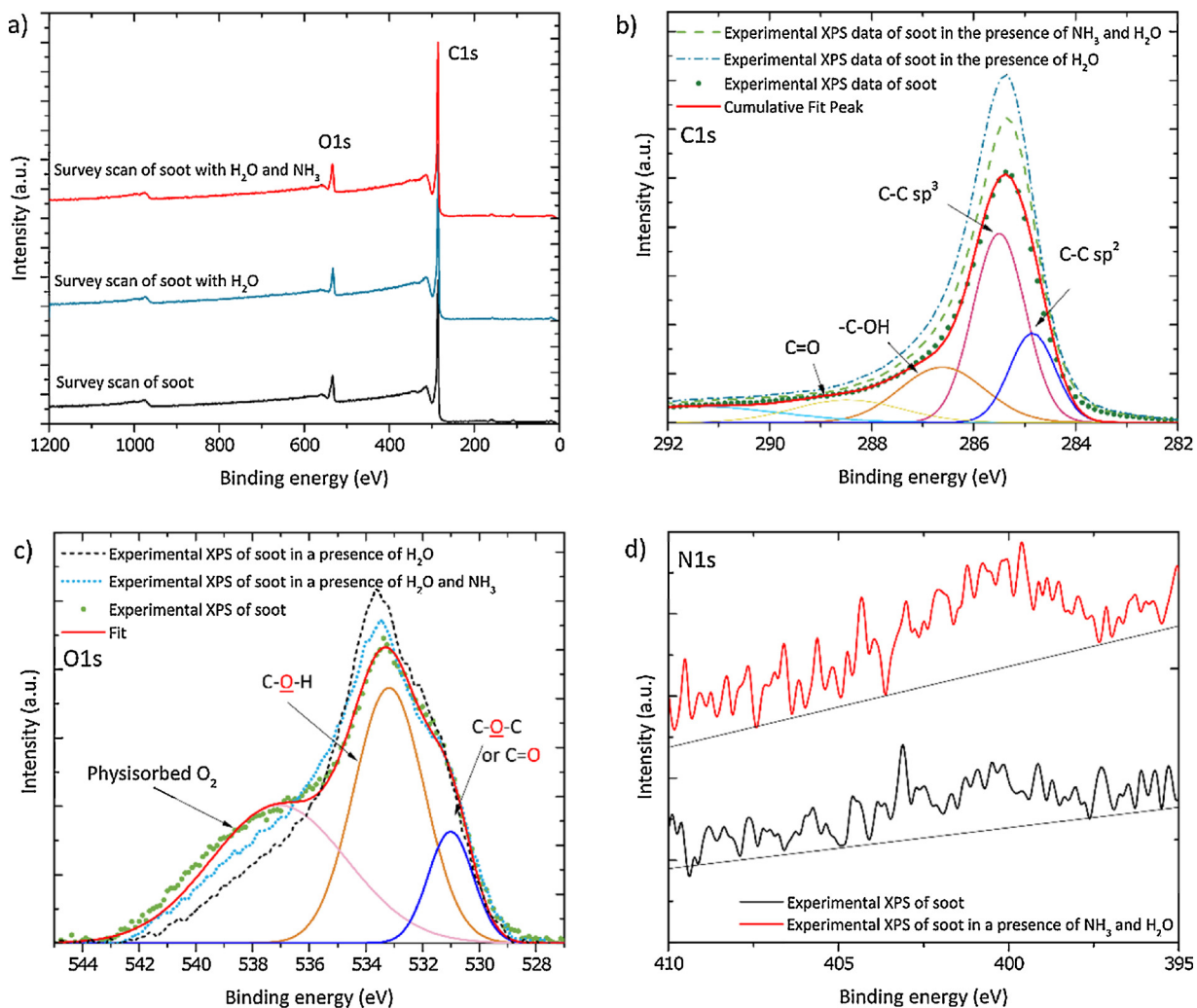


**Fig. 4.** XPS investigation of the interaction of NH<sub>3</sub> and H<sub>2</sub>O with soot. The soot, soot with H<sub>2</sub>O and soot with H<sub>2</sub>O and NH<sub>3</sub> are shown in a) Survey scan b) C1s spectra with deconvolution of soot results c) O1s spectra with deconvolution results for soot spectrum and d) N1s spectra.

particles can be seen in the SEM image in Fig. S1 (Supplementary material).

Bhatia and Perlmutter [41] have developed a model, proposed by Gavals [40], that considers the growth of pores with random pore size distribution and incorporates the growth of the specific surface area

(S<sub>a</sub>) of soot as a function of the carbon coverage θ<sub>c</sub>. This behaviour has been documented in experiments by Ishiguro et al. [94]. The expression for specific surface area in the Bhatia and Perlmutter model [41,46] is

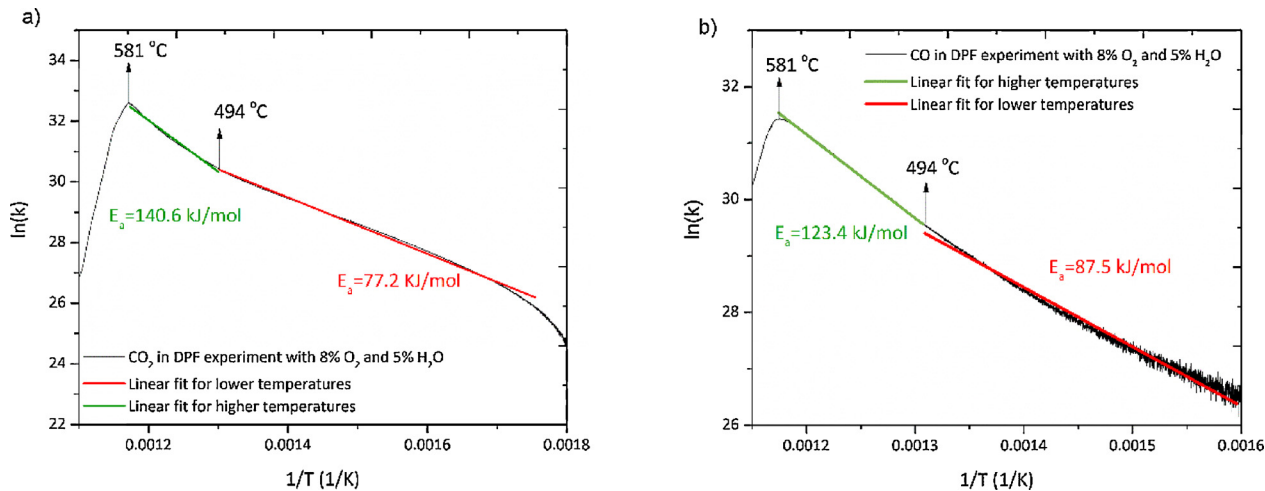


**Fig. 5.** Activation energies for a) CO<sub>2</sub> and b) CO production for soot oxidation on DPF.

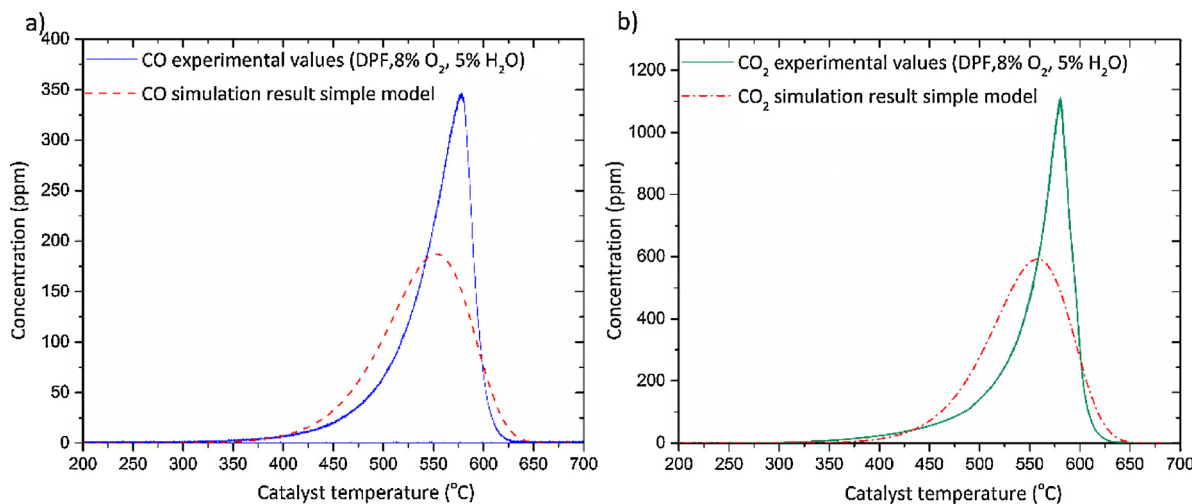


**Fig. 6.** Experimental and simulation results, using the simple model (see R.1 and R.2 in Table 1) for soot oxidation on DPF in the presence of 8% O<sub>2</sub> and 5% H<sub>2</sub>O.

**Table 1**

Parameters for the kinetic model for soot oxidation in the presence of H<sub>2</sub>O and O<sub>2</sub>.

Reactions	Reaction rate simple model	A <sub>i</sub> (s <sup>-1</sup> )	E <sub>a</sub> (kJ/mol)	Reaction N°
C + O <sub>2</sub> → CO <sub>2</sub>	r <sub>CO2</sub> = ψ <sub>C</sub> k <sub>CO2</sub> y <sub>O2</sub> θ <sub>C</sub>	5.05×10 <sup>6</sup>	140.6	R.1
C + $\frac{1}{2}$ O <sub>2</sub> → CO	r <sub>CO</sub> = ψ <sub>C</sub> k <sub>CO</sub> y <sub>O2</sub> θ <sub>C</sub>	1.3×10 <sup>5</sup>	123.4	R.2

$$S_a = S_{a0}\theta_c \sqrt{1-\Psi} \ln(\theta_c) \quad (11)$$

where S<sub>a0</sub> is the initial surface area. The structural factor that describes pore structure is Ψ. For Ψ > 2, the specific surface area first grows with a pore opening, and, after reaching a maximum, starts promptly to decrease as pore walls collapse into each other as the reaction proceeds. The reaction rate according to Bhatia and Perlmutter model [41,46] is

$$r = A\theta_c \sqrt{1-\Psi} \ln(\theta_c) \exp(-E_a/RT) p_{O2}^n \quad (12)$$

where p<sub>O2</sub> is the partial pressure of oxygen. The random pore model (RPM) showed very good agreement with experimental data [90,91,98–100].

We, therefore, investigated a random pore model for our system, and the reactions and rates are presented in Table 2 (R.3 and R.4). The activation energies are from experimental data (Fig. 5) while the pre-exponential factors and Ψ were manually fitted. The fitted Ψ value result is 10, which means growth in a specific surface area during soot combustion as a consequence of porous soot. The maximum increase in surface area (S<sub>a</sub>/S<sub>a0</sub>), using Eq. (12), was 1.498 for Ψ = 10, as presented in Fig. S6 in the supplementary material. The initial increase in specific surface area means an increase at the active sites [46]. For a conversion larger than 0.327, the surface decreases more rapidly due to the collapse of the pores. This means that soot oxidation occurs at more narrow temperature intervals. The results of this model are shown in Fig. 7, and it is clear that the random pore model describes the experimental features well.

**Table 2**

Reaction and rates for the random pore kinetic model for soot oxidation in the presence of H<sub>2</sub>O and O<sub>2</sub> using DPF.

Reactions	Reaction rate simple model	A <sub>i</sub> (s <sup>-1</sup> )	E <sub>a</sub> (kJ/mol)	Ψ	Reaction N°
C + O <sub>2</sub> → CO <sub>2</sub>	r <sub>CO2</sub> = ψ <sub>C</sub> k <sub>CO2</sub> y <sub>O2</sub> θ <sub>C</sub> √(1-Ψln(θ <sub>C</sub> ))	1.3×10 <sup>6</sup>	140.6	10	R.3
C + $\frac{1}{2}$ O <sub>2</sub> → CO	r <sub>CO</sub> = ψ <sub>C</sub> k <sub>CO</sub> y <sub>O2</sub> θ <sub>C</sub> √(1-Ψln(θ <sub>C</sub> ))	0.4×10 <sup>5</sup>	123.4	10	R.4

#### 4.4.2. Kinetic model for the NH<sub>3</sub> effect on soot oxidation over DPF

The results from DRIFT and XPS measurements were used to incorporate the negative effect of NH<sub>3</sub> (Fig. 1) on soot oxidation. The appearance of amines, or amide groups, after NH<sub>3</sub>, was incorporated in Reaction R.5, see Table 3. In the experiment over DPF, there was clear ammonia consumption and, at the same time, NO production. For this reason, we added a global reaction step in which the amines group was oxidized to form NO (R.6 in Table 3). These amines, or an amides group, block the soot and, thereby, reduce the oxidation capacity.

The results of this model are shown together with the experiments for CO and CO<sub>2</sub> in Fig. 8a and, for NH<sub>3</sub> and NO in Fig. 8b. The grey area in the Figure marks the difference between the temperature for maximum CO<sub>x</sub> production for experiment and simulation. As can be seen, the shape of the peaks corresponds well with the experimental result, but the position of the simulated CO and CO<sub>2</sub> peaks, as well as NH<sub>3</sub> consumption and NO production are at significantly lower temperatures in the model. We suggest that the negative influence of NH<sub>3</sub> on soot oxidation comes from blockages of carbons with amines, or an amides, but, in this case, the mechanism with which one amine, or an amide group, blocks one carbon was not sufficient. This was because the simulation showed soot oxidation at a significantly lower temperature. The CO and CO<sub>2</sub> peaks were, therefore, integrated, and the amount of carbons oxidized were compared to the number of NH<sub>3</sub> molecules consumed on the soot surface, giving the value of 0.63 mmol of NH<sub>3</sub> and 7.5 mmol of soot in 350–650 °C temperature range, which resulted in a molar ratio of around 12. This means that one ammonia molecule blocks about 12 carbon atoms on average.

Many studies that try to explain the complex phenomenon of soot oxidation suggested that the average soot oxidation takes place through the active surface or "free-edge" sites [101–104]. The main principle is to simplify the complex soot structure with one surface carbon called a "free-edge" site, which has greater reactivity than the surrounding carbons [105–107]. One carbon is the starting point of soot oxidation with step-by-step behaviour [103]. We, therefore, propose that the reason there is such a large blockage of soot oxidation and, at the same time, quite low ammonia consumption, is that NH<sub>3</sub> blocks these reactive free-

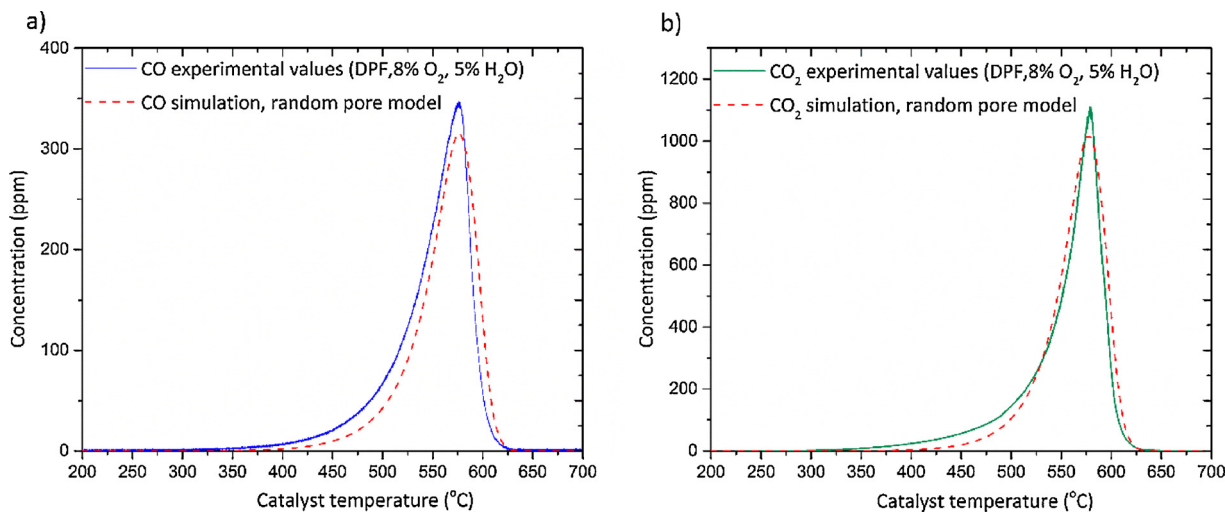


**Fig. 7.** Experimental and simulation results, using the random pore model (see Reactions R.3 and R.4 in Table 2) for soot oxidation on DPF in the presence of 8% O<sub>2</sub> and 5% H<sub>2</sub>O.

**Table 3**

Reactions, reaction rates and parameters for the random pore kinetic model for soot oxidation in the presence of NH<sub>3</sub>, H<sub>2</sub>O and O<sub>2</sub>.

Reactions and Reaction rate	A <sub>i</sub> (s <sup>-1</sup> )	E <sub>a</sub> (kJ/mol)	Reaction N°
2C + 2NH <sub>3</sub> + $\frac{1}{2}$ O <sub>2</sub> → 2C-NH <sub>2</sub> + H <sub>2</sub> O	0.4×10 <sup>6</sup>	91.0	R.5
r <sub>NH2</sub> = $\psi_C k_{NH2} y_{NH3} y_{O2} \theta_C$			
2C-NH <sub>2</sub> + 4O <sub>2</sub> → 2CO <sub>2</sub> + 2NO + 2H <sub>2</sub> O	2×10 <sup>4</sup>	105.0	R.6
r <sub>CO</sub> = $\psi_C k_C y_{O2} \theta_C$			

edge sites. This results in blocking not just one site of carbon but also the group of carbons connected to the starting carbon site. For this reason, we incorporated the mechanism of free-edge sites into the kinetic model and the adsorption of ammonia on these reactive free-edge sites. To do so, a global model was developed in which certain amount of carbons were lumped into one F-site, which means that these carbons could only react if the free-edge site reacted. This is described by adding Reaction R.7 in Table 4.

In addition to NH<sub>3</sub>, water vapor was also present in our system. It is well documented that water promotes soot oxidation [108–111]. We also observed OH groups both with XPS measurements (Fig. 4) and with *in-situ* DRIFT (Fig. 3). For this reason, we introduced the formation of OH groups on the reactive free-edge site (F). This reaction is shown in

**Table 4**

Parameters for the kinetic model for soot oxidation in the presence of H<sub>2</sub>O and O<sub>2</sub>.

Reactions and Reaction rates	A <sub>i</sub> (s <sup>-1</sup> )	E <sub>a</sub> (kJ/mol)	Reaction N°
x•C → F	10 <sup>10</sup>	0	R.7
r <sub>F</sub> = $\psi_C k_F \theta_C$			
2F + H <sub>2</sub> O + $\frac{1}{2}$ O <sub>2</sub> → 2F-OH	10 <sup>5</sup>	10.0	R.8
r <sub>F-OH</sub> = $\psi_C k_{F-OH} y_{H2O} y_{O2} \theta_F$			
2F-OH → CO + H <sub>2</sub> O + (2x-1)C	3.2×10 <sup>3</sup>	123.4	R.9
r <sub>F-CO</sub> = $\psi_C k_{F-CO} \theta_{F-OH} \sqrt{1-\Psi ln(\theta_{F-OH})}$			
2F-OH + $\frac{1}{2}$ O <sub>2</sub> → CO <sub>2</sub> + H <sub>2</sub> O + (2x-1)C	1.4×10 <sup>6</sup>	140.6	R.10
r <sub>F-CO<sub>2</sub></sub> = $\psi_C k_{F-CO2} y_{O2} \theta_{F-OH} \sqrt{1-\Psi ln(\theta_{F-OH})}$			

**Table 4** (R.8). The OH group on the reactive F-site is suggested to interact with NH<sub>3</sub> and form amines, or an amide group, which was also detected in the DRIFT measurement (Fig. 3). This is in line with the mechanism proposed by Wolff and Klimisch [76]. A schematic representation of the OH groups and their interaction with ammonia to produce amides are shown in Fig. 9.

By manual tuning, we observed that about 15 carbons, on average,

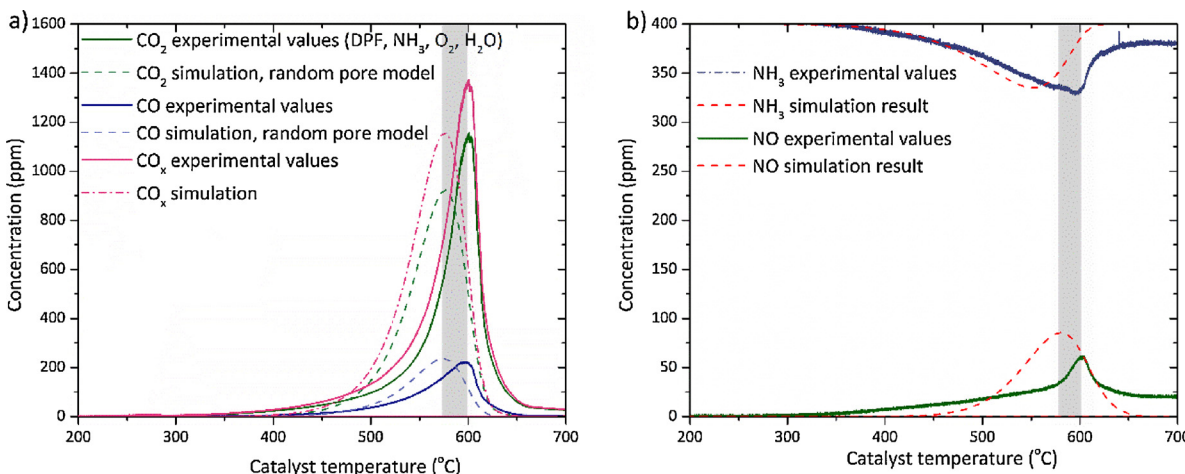


**Fig. 8.** Experimental and simulation result, for soot and NH<sub>3</sub> oxidation over DPF using reaction R.5 and R.6 (Table 3) in the presence of 400 ppm NH<sub>3</sub>, 8% O<sub>2</sub> and 5% H<sub>2</sub>O. The grey area marks the difference between the temperature for maximum CO<sub>x</sub> production for experiment and simulation.

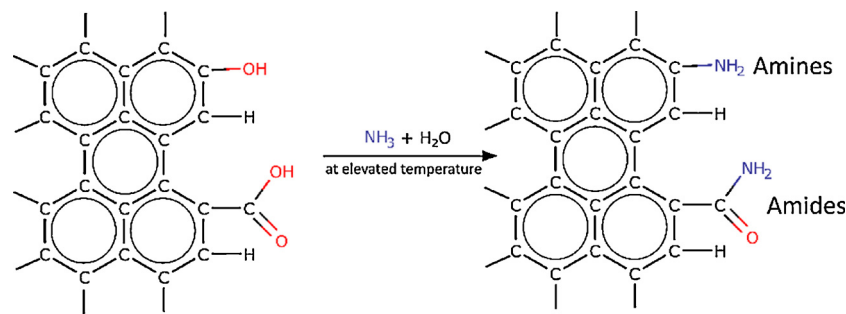


**Fig. 9.** Chemical structure of interaction of soot with  $\text{NH}_3$  in the presence of water. Partially redrawn from [76].

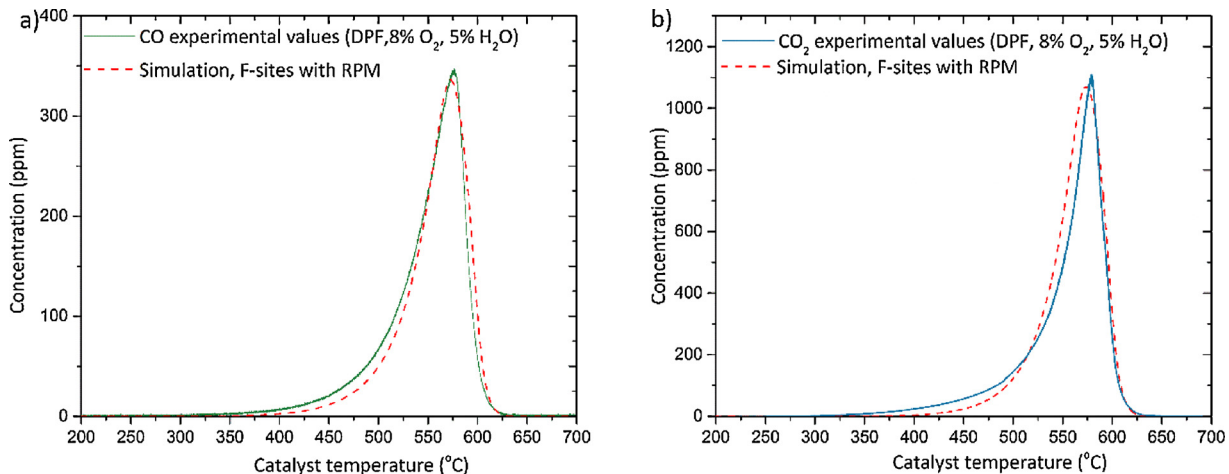


**Fig. 10.** Experimental and simulation results, for soot oxidation on DPF using F-equation together with random pore model (Reactions R.7-R.10, Table 4) in the presence of 8%  $\text{O}_2$  and 5%  $\text{H}_2\text{O}$ .

**Table 5**  
Reactions and rates for the free-edge sites kinetic model for soot oxidation over DPF in the presence of  $\text{NH}_3$ ,  $\text{H}_2\text{O}$  and  $\text{O}_2$ .

Reactions and Reaction rates	$A_i (\text{s}^{-1})$	$E_a (\text{kJ/mol})$	Reaction N°
$\text{F-OH} + \text{NH}_3 \rightarrow \text{F-NH}_2 + \text{H}_2\text{O}$	$13 \times 10^4$	94.0	R.11
$r_{\text{F}-\text{NH}_2} = \psi_C k_{\text{F}-\text{NH}_2} \theta_{\text{F}-\text{OH}}$			
$3 \text{F-NH}_2 + 2 \text{O}_2 \rightarrow 3 \text{F} + \text{NO} + \text{H}_2\text{O} + \text{N}_2$	$2 \times 10^7$	172.0	R.12
$r_{\text{NO}} = \psi_C k_{\text{F}-\text{NH}_2} \gamma_{\text{O}_2} \theta_{\text{F}-\text{NH}_2}$			

must be associated with this F-site ( $F = 15\text{C}$ ) in order to capture the ammonia inhibition effect. The model using free edge sites was first tested for soot oxidation in the presence of  $\text{O}_2$  and  $\text{H}_2\text{O}$ , and the random pore model was used to incorporate the morphology change in soot particles using Reactions R.9 and R.10, see Table 4. Fig. 10 shows the results of the simulation compared with the experimental data for soot oxidation in the presence of 8% and 5%  $\text{H}_2\text{O}$  for the parameters listed in Table 4. As can be seen in the figure, the shape and the position of the simulated peaks for CO and  $\text{CO}_2$  correspond well to our experimental data.

Reaction R.11 in Table 5 was added to the model to describe the

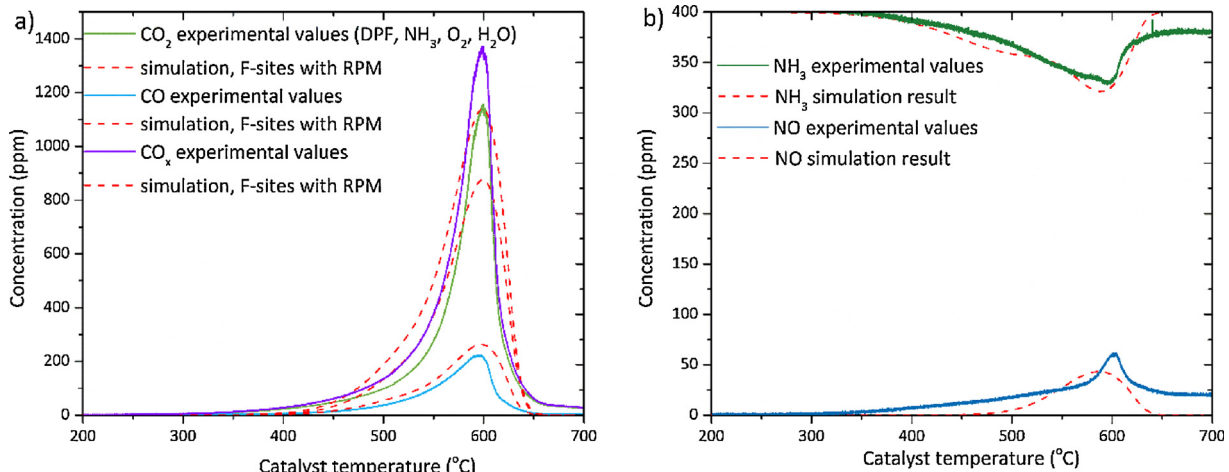


**Fig. 11.** Experimental and simulation results for soot and  $\text{NH}_3$  oxidation over a DPF using parameters from Equations R.7-R.12 in the presence of 400 ppm  $\text{NH}_3$ , 8%  $\text{O}_2$ , and 5%  $\text{H}_2\text{O}$ .

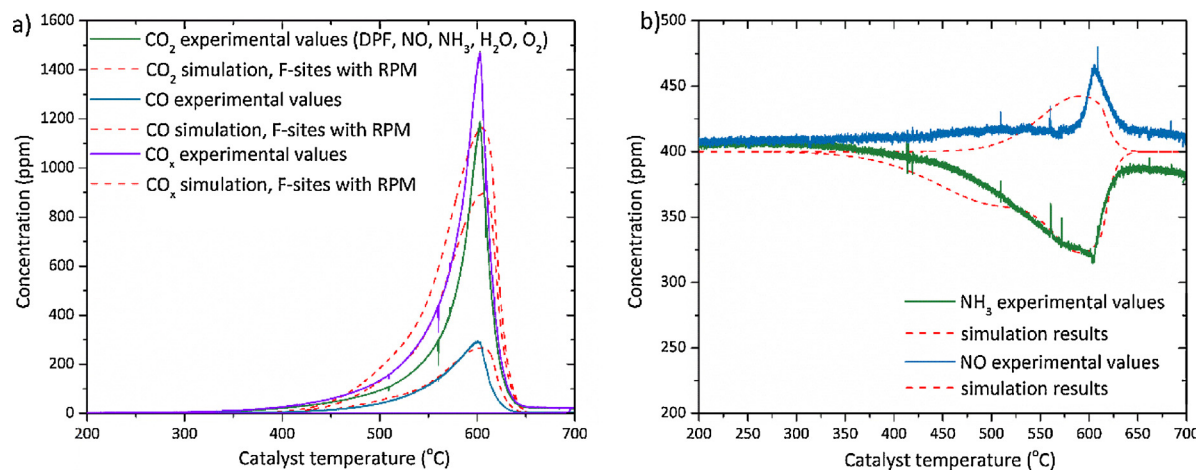


**Fig. 12.** Experimental and simulation results, for soot oxidation and NH<sub>3</sub> oxidation on DPF using parameters from Equations R.7-R.12 in the presence of 400 ppm NH<sub>3</sub>, 400 ppm NO, 8% O<sub>2</sub> and 5% H<sub>2</sub>O.

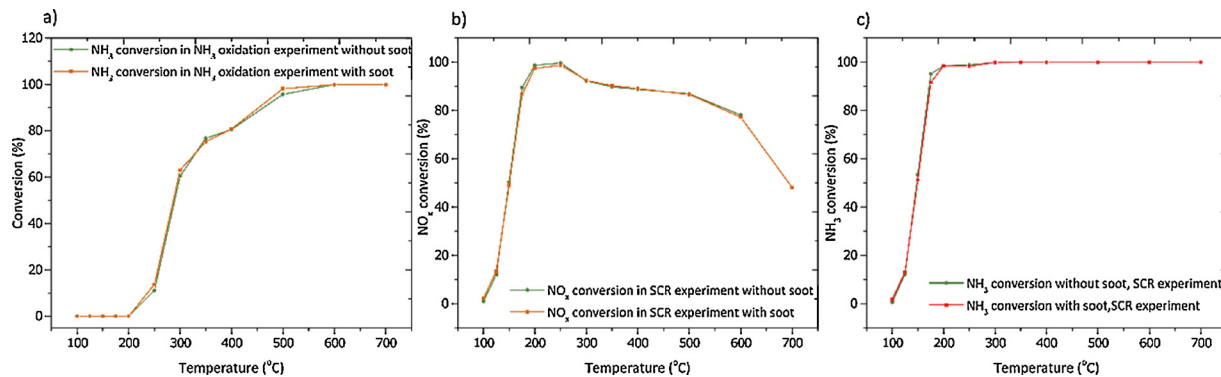


**Fig. 13.** a) NH<sub>3</sub> conversion for NH<sub>3</sub> oxidation experiments b) NO<sub>x</sub> and c) NH<sub>3</sub> conversion for NH<sub>3</sub>-SCR experiments over Cu/SSZ13 with and without soot loading.

**Table 6**

Reactions and parameters for kinetic model for soot oxidation using free edge sites in the presence of H<sub>2</sub>O, O<sub>2</sub>, and NH<sub>3</sub> over soot impregnated Cu/SSZ-13. Rate expressions can be found in Tables 4 and 5.

Reactions	A <sub>i</sub> (s <sup>-1</sup> )	E <sub>a</sub> (kJ/mol)	Reaction N°
xC → F	10 <sup>10</sup>	0	R.7
2F + H <sub>2</sub> O + $\frac{1}{2}$ O <sub>2</sub> → 2F-OH	10 <sup>5</sup>	10.0	R.8
2F-OH → CO + H <sub>2</sub> O + (2x-1)C	2.3 × 10 <sup>3</sup>	123.4	R.9
2F-OH + $\frac{1}{2}$ O <sub>2</sub> → CO <sub>2</sub> + H <sub>2</sub> O + (2x-1)C	7.8 × 10 <sup>6</sup>	140.6	R.10
F-OH + NH <sub>3</sub> → F-NH <sub>2</sub> + H <sub>2</sub> O	13 × 10 <sup>4</sup>	86.0	R.11
3F-NH <sub>2</sub> + 2O <sub>2</sub> → 3F + NO + H <sub>2</sub> O + N <sub>2</sub>	1.38 × 10 <sup>7</sup>	170.0	R.12

interaction between NH<sub>3</sub> and the OH groups in forming amines or an amide. Since it was observed that ammonia was consumed during soot oxidation and that NO was formed simultaneously, we added one additional reaction to describe this (see Reaction R.12 in Table 5). The parameters for the formation of CO and CO<sub>2</sub> (Reaction R.7-R.10, Table 4) were used together with Reactions R.11 and R.12 (Table 5) to simulate soot oxidation in the presence of NH<sub>3</sub>, O<sub>2</sub>, and H<sub>2</sub>O. The simulated results for CO, CO<sub>2</sub>, NH<sub>3</sub>, and NO are compared with experimental data and presented in Fig. 11. The model describes the experimental features well. It is clear that the simulation results (compare Figs. 8 and 11) significantly improves when the free edge site model was added, since it now predict the delayed soot oxidation due to the presence of NH<sub>3</sub> well.

The model was also used for soot oxidation over DPF in NH<sub>3</sub>-SCR conditions in the presence of 400 ppm NH<sub>3</sub>, 400 ppm NO, 8% O<sub>2</sub>, and

5% H<sub>2</sub>O, and the results are shown in Fig. 12. The model also describes this experiment well.

#### 4.5. A kinetic model for an SCR coated filter

The effect of soot on ammonia oxidation over Cu/SSZ-13 was studied by exposing the catalyst, with or without soot, to 400 ppm NH<sub>3</sub>, 8% O<sub>2</sub> and 5% H<sub>2</sub>O and increasing the temperature stepwise from 100 to 600 °C. The results for NH<sub>3</sub> conversion with and without soot are presented in Fig. 13a. As can be seen in the figure, the conversion of NH<sub>3</sub> started at 250 °C with full NH<sub>3</sub> conversion from 600 °C. No effect of soot on ammonia oxidation was observed. The results of NO<sub>x</sub> and NH<sub>3</sub> conversion in the NH<sub>3</sub>-SCR experiment on a Cu/SSZ-13 sample with and without soot are shown in Fig. 13b and c, respectively. The feed consisted of 400 ppm NO, 400 ppm NH<sub>3</sub>, 8% O<sub>2</sub>, and 5% H<sub>2</sub>O. As shown in the figure, there was no conversion of NO<sub>x</sub> or NH<sub>3</sub> at 100 °C, and full conversion of NO<sub>x</sub> is observed at 200 °C. Because the onset of ammonia oxidation for temperatures higher than 200 °C conversion of NO<sub>x</sub> for NH<sub>3</sub>-SCR decreases. These results show that soot had no or only a minor effect on the ammonia oxidation and the SCR reactions using soot loading of 10 g/l. It should be noted that during the course of the experiment the soot loading will decrease at higher temperature due to soot oxidation.

As described in Introduction section, an SCR coated filter is a technology that combines both a particulate filter and an SCR catalyst. In this study, we used Cu/SSZ-13 impregnated with soot to mimic an SCR coated filter. We create the SCR filter model as a combination of the kinetic models for Cu/SSZ-13 and the DPF model developed in Subsection 4.4. First the reactions for NH<sub>3</sub> storage, NH<sub>3</sub> oxidation and

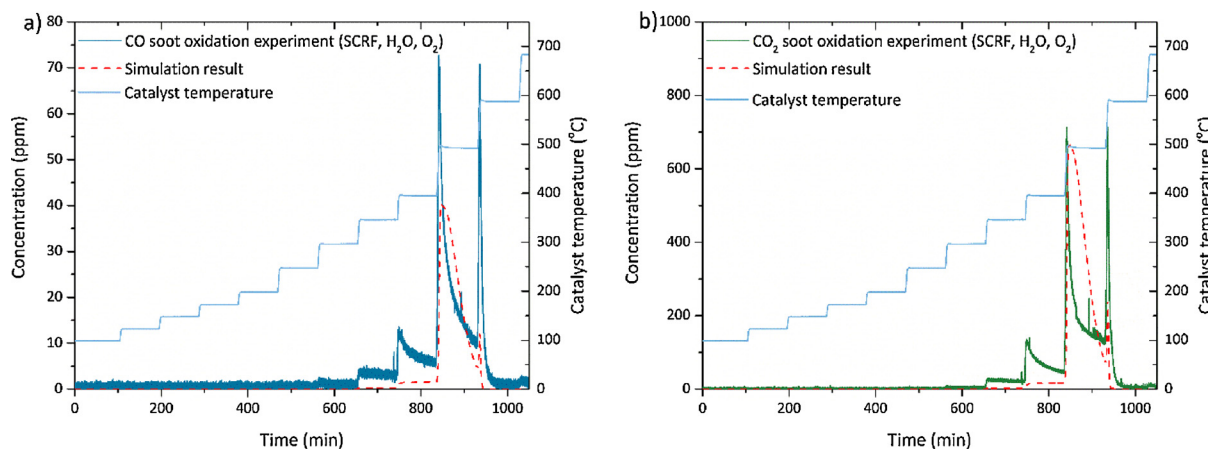


**Fig. 14.** Experimental and simulation result, for soot oxidation on soot impregnated Cu/SSZ-13 using parameters from reactions R.7-R.10, Table 6 in the presence of 8% O<sub>2</sub> and 5% H<sub>2</sub>O.

NH<sub>3</sub> SCR from the model by Olsson et al. [21] were tuned to our experiments over Cu/SSZ-13. Parameters, together with reactions and rates, are listed in Supplementary material in Table S1. The N<sub>2</sub>O and NO<sub>2</sub> production for NH<sub>3</sub> oxidation and NH<sub>3</sub> SCR experiments were not included in the model, since these were low in the experiments (maximum 12 ppm), see Figure S7. The experiments shown in Fig. 13 with Cu/SSZ-13 impregnated with soot were used to simulate of the SCR coated filters. The temperature measured in the gas phase before the monolith was used in the simulations.

Reactions for soot oxidation in the presence of 8% O<sub>2</sub> and 5% H<sub>2</sub>O (R.7-R.10, Table 4) were used together with the SCR model. However, it was observed that the Cu/SSZ-13 catalyst slightly changed the rates for soot oxidation. The pre-exponential factors for the soot oxidation reaction were, therefore, tuned somewhat and the new parameters are shown in Table 6 (R.9 and R.10). Some minor adjustments to the parameters in Reactions R.11 and R.12 were also needed (see Table 6). Overall, the same reactions and rates as were developed for the DPF (Reactions R.7-R.10, Table 4) were used to model soot oxidation over Cu/SSZ-13, but with minor modifications of the parameters, as shown in Table 6. A comparison between simulated and experimental data is shown in Fig. 14 for the experiment with soot oxidation in the presence of O<sub>2</sub> and H<sub>2</sub>O over Cu/SSZ-13. The model described CO and CO<sub>2</sub> production adequately when the temperature was increased stepwise. However, in the experiment there was some soot oxidized also at lower temperature (350–400 °C), which the model did not predict. The reason for this could be that some soot might be very close to the catalytical active sites, while some are not. This could cause a distribution of soot

oxidation activity, but this feature was not added to the model, in order not to complicate the model further.

The model was further used for ammonia oxidation and SCR experiments with the Cu/SSZ-13 monolith impregnated with soot. These results are shown in Figs. 15 and 16, respectively. It is clear in the figures that the developed model describes well both the soot reactions and the SCR reactions over the soot impregnated SCR catalyst.

## 5. Conclusions

The effect of soot loading on a Cu/SSZ-13 zeolite in standard SCR, NH<sub>3</sub> oxidation, NH<sub>3</sub> TPD, and soot oxidation was studied. The SCR experiment, and ammonia oxidation showed that the activity of Cu/SSZ-13 was not influenced by the presence of soot using a soot loading of 10 g/l. Soot oxidation in the presence of ammonia revealed that soot oxidation was lowered, which shows an interaction between soot and ammonia. In ammonia SCR conditions, the activity for soot oxidation was regained near 500 °C. This can be explained by the fact, that at this high temperature, the SCR zone is very short, for the reason, the majority of the catalyst is not exposed to ammonia, and therefore the inhibition effect of ammonia was not observed.

Ammonia TPD experiments were used to investigate ammonia storage and the effect of soot. The results indicated that there were an interaction between soot and NH<sub>3</sub>. To further study this, *in-situ* DRIFT and XPS experiments were performed. The *in-situ* DRIFT spectroscopy showed amines and/or amide-species after exposing soot to gas containing ammonia. The XPS showed the existence of OH groups as well

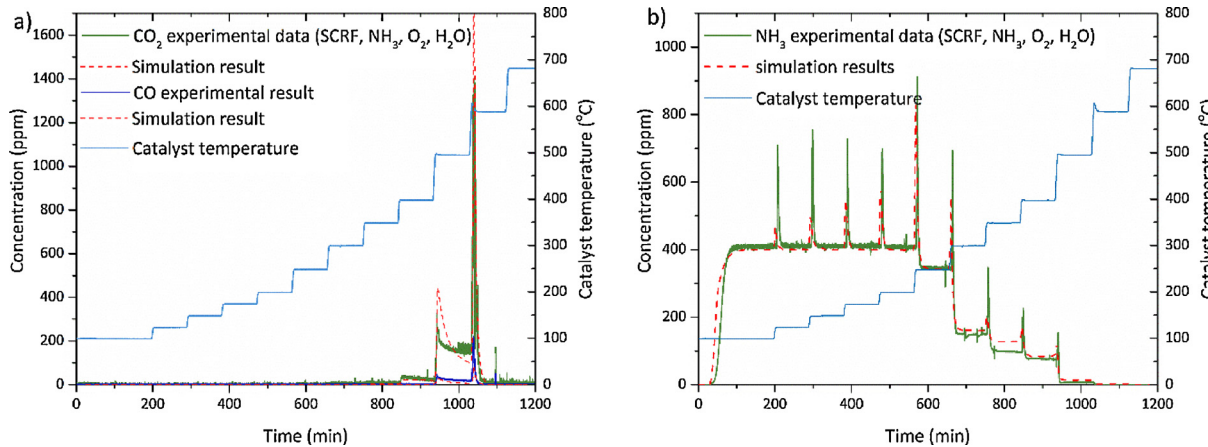


**Fig. 15.** Experimental and simulation results, for soot oxidation on soot impregnated Cu/SSZ-13 using Reactions R.7-R.12, (Table 6) for soot and SCR reactions in Table S.1 for Cu/SSZ-13 in the presence of 400 ppm NH<sub>3</sub>, 8% O<sub>2</sub>, and 5% H<sub>2</sub>O.

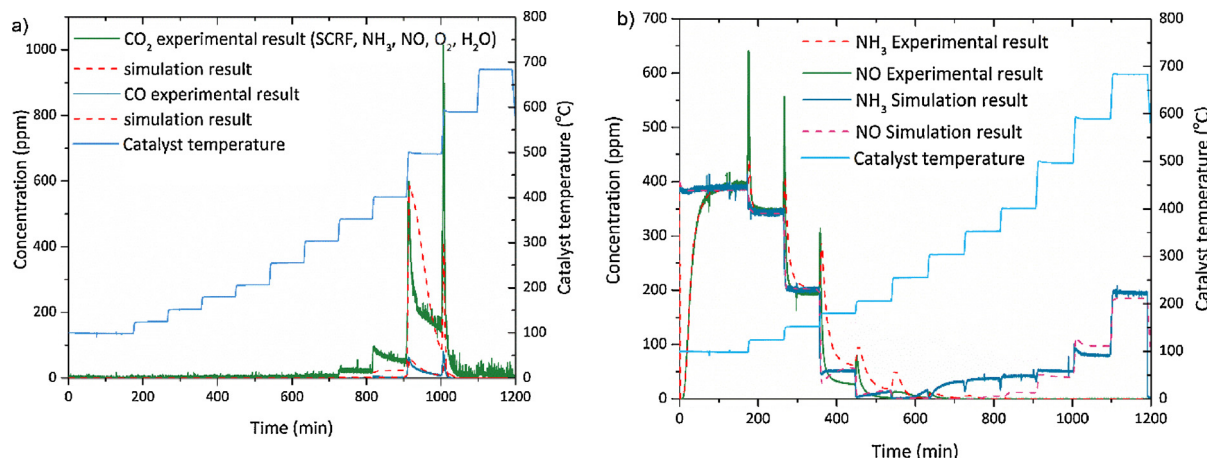


**Fig. 16.** Experimental and simulation results, for soot oxidation on soot impregnated Cu/SSZ-13 using Reactions R.7-R.12, (Table 6) for soot and SCR reactions in Table S.1 for Cu/SSZ-13 in the presence of 400 ppm NH<sub>3</sub>, 400 ppm NO, 8% O<sub>2</sub> and 5% H<sub>2</sub>O.

as a small amount of NH<sub>2</sub> groups on the surface of the soot after it was treated with H<sub>2</sub>O and NH<sub>3</sub> prior to XPS measurements. The flow reactor experiments combined with the results from *in-situ* DRIFT and XPS clearly show that there was an interaction between soot and NH<sub>3</sub>.

The experimental results were used to develop a kinetic models for soot oxidation on DPF and an SCR coated filter in the presence of different gases. Soot oxidation on the DPF sample, where the sample was exposed to water and oxygen and the temperature was linearly increased, was used as the base for the development of a model for soot oxidation. Initially a simple model was investigated, however, this simplified model could not describe the results adequately. It gave a CO<sub>x</sub> peak in the simulation that was too broad compared to the experiment. A random pore model was, therefore, used, which gave good results. This model was used in the subsequent simulations. As already mentioned, ammonia had a clear inhibiting effect on soot oxidation over DPF and also on the SCR coated filter. *In-situ* DRIFT spectroscopy showed that amines and/or amide species (C-NH<sub>2</sub>) formed, and it is possible that these amine and amide species blocked soot oxidation. Therefore, a reaction step was added in which C-NH<sub>2</sub> was formed, and reacted further to produce NO. However, this model could not predict the large increase in light off temperature observed, with the simultaneous low consumption of ammonia. Mechanisms describing soot oxidation that starts on free edge carbons have been found in the literature, that considers that not all carbons are equally reactive. We, therefore, incorporated into our kinetic model a mechanism with which ammonia blocked these free edge carbon sites. The model could, thereafter, describe the shift in oxidation temperature well. The next step was to simulate ammonia SCR conditions over the DPF, and the model also described those results well.

A kinetic model for ammonia storage/desorption, ammonia oxidation, and ammonia SCR was tuned to the experimental data using a Cu/SSZ-13 catalyst, and the model could describe the SCR functionalities over a broad temperature range. The SCR model, the random pore model, and the ammonia inhibition of free edge carbon sites were combined, and the model described well ammonia SCR activity over a soot loaded Cu/SSZ-13 sample, including soot regeneration.

## Acknowledgments

This research was conducted within the REWARD project: REal World Advanced Technologies foR Diesel Engines. This project has received funding from the European Unions Horizon 2020 research and innovation programme under grant agreement No 636380.

## Appendix A. Supplementary data

Supplementary data associated with this article can be found, in the online version, at <https://doi.org/10.1016/j.apcatb.2018.08.076>.

## References

- [1] D. Fino, S. Bensaid, M. Piumetti, N. Russo, A review on the catalytic combustion of soot in Diesel particulate filters for automotive applications: from powder catalysts to structured reactors, *Appl. Catal. A* 509 (2016) 75–96.
- [2] T.V. Johnson, Review of diesel emissions and control, *SAE Int. J. Fuels Lubr.* 3 (2010) 16–29.
- [3] Urea-SCR Technology for deNOx After Treatment of Diesel Exhausts, Springer, New York, 2014.
- [4] B. Guan, R. Zhan, H. Lin, Z. Huang, Review of state of the art technologies of selective catalytic reduction of NOx from diesel engine exhaust, *Appl. Therm. Eng.* 66 (2014) 395–414.
- [5] A. Russell, W.S. Epling, Diesel oxidation catalysts, *Catal. Rev.* 53 (2011) 337–423.
- [6] A. Lundstrom, B. Andersson, L. Olsson, Urea thermolysis studied under flow reactor conditions using DSC and FT-IR, *Chem. Eng. J.* 150 (2009) 544–550.
- [7] X. Song, J.H. Johnson, J.D. Naber, A review of the literature of selective catalytic reduction catalysts integrated into diesel particulate filters, *Int. J. Engine Res.* 16 (2015) 738–749.
- [8] K.G. Rappé, Integrated selective catalytic reduction-diesel particulate filter aftertreatment: insights into pressure drop, NOx conversion, and passive soot oxidation behavior, *Ind. Eng. Chem. Res.* 53 (2014) 17547–17557.
- [9] J.H. Lee, M.J. Paratore, D.B. Brown, Evaluation of Cu-based SCR/DPF technology for diesel exhaust emission control, *SAE Int. J. Fuels Lubr.* 1 (2008) 96–101.
- [10] J. Czerwinski, Y. Zimmerli, A. Mayer, G. D'Urbano, D. Zürcher, Emission reduction with diesel particle filter with SCR coating (SDPF), *Emiss. Control Sci. Technol.* 1 (2015) 152–166.
- [11] Y.M. López De Jesús, P.I. Chigada, T.C. Watling, K. Arulraj, A. Thorén, N. Greenham, P. Markatou, NOx and PM Reduction from Diesel Exhaust Using Vanadia SCR®, *SAE Int. J. Engines* 9 (2016) 1247–1257.
- [12] L. Cumaranatunge, A. Chiffey, J. Stetina, K. McGonigle, G. Repley, A. Lee, S. Chatterjee, A study of the soot combustion efficiency of an SCR® catalyst vs a CSF during active regeneration, *Emiss. Control Sci. Technol.* 3 (2017) 93–104.
- [13] K. Leistner, O. Mihai, K. Wijayanti, A. Kumar, K. Kamasamudram, N.W. Currier, A. Yezerets, L. Olsson, Comparison of Cu/BEA, Cu/SSZ-13 and Cu/SAPO-34 for ammonia-SCR reactions, *Catal. Today* 258 (2015) 49–55.
- [14] L. Xie, F. Liu, L. Ren, X. Shi, F.-S. Xiao, H. He, Excellent performance of one-pot synthesized Cu-SSZ-13 catalyst for the selective catalytic reduction of NOx with NH<sub>3</sub>, *Environ. Sci. Technol.* 48 (2014) 566–572.
- [15] S. Han, Q. Ye, S. Cheng, T. Kang, H. Dai, Effect of the hydrothermal aging temperature and Cu/Al ratio on the hydrothermal stability of CuSSZ-13 catalysts for NH<sub>3</sub>-SCR, *Catal. Sci. Technol.* 7 (2017) 703–717.
- [16] Q. Ye, L. Wang, R.T. Yang, Activity, propene poisoning resistance and hydrothermal stability of copper exchanged chabazite-like zeolite catalysts for SCR of NO with ammonia in comparison to Cu/ZSM-5, *Appl. Catal. A Gen.* 427–428 (2012) 24–34.
- [17] J.H. Kwak, R.G. Tonkyn, D.H. Kim, J. Szanyi, C.H.F. Peden, Excellent activity and selectivity of Cu-SSZ-13 in the selective catalytic reduction of NOx with NH<sub>3</sub>, *J. Catal.* 275 (2010) 187–190.
- [18] Z. Zhao, R. Yu, R. Zhao, C. Shi, H. Gies, F.-S. Xiao, D. De Vos, T. Yokoi, X. Bao, U. Kolb, M. Feyen, R. McGuire, S. Maurer, A. Moini, U. Müller, W. Zhang, Cu-exchanged Al-rich SSZ-13 zeolite from organotemplate-free synthesis as NH<sub>3</sub>-SCR catalyst: Effects of Na<sup>+</sup> ions on the activity and hydrothermal stability, *Appl. Catal. B* 217 (2017) 421–428.

- [19] R. Zhang, N. Liu, Z. Lei, B. Chen, Selective transformation of various nitrogen-containing exhaust gases toward  $N_2$  over zeolite catalysts, *Chem. Rev.* 116 (2016) 3658–3721.
- [20] D.W. Fickel, E.D. Addio, J.A. Lauterbach, R.F. Lobo, The ammonia selective catalytic reduction activity of copper-exchanged small-pore zeolites, *Appl. Catal. B* 102 (2011) 441–448.
- [21] L. Olsson, K. Wijayanti, K. Leistner, A. Kumar, S.Y. Joshi, K. Kamasamudram, N.W. Currier, A. Yezersets, A multi-site kinetic model for NH<sub>3</sub>-SCR over Cu/SSZ-13, *Appl. Catal. B* 174–175 (2015) 212–224.
- [22] H. Sjövall, R.J. Blint, L. Olsson, Detailed kinetic modeling of NH<sub>3</sub> SCR over Cu-ZSM-5, *Appl. Catal. B* 92 (2009) 138–153.
- [23] M. Colombo, I. Nova, E. Tronconi, Detailed kinetic modeling of the NH<sub>3</sub>-NO/NO<sub>x</sub> SCR reactions over a commercial Cu-zeolite catalyst for Diesel exhausts after treatment, *Catal. Today* 197 (2012) 243–255.
- [24] M. Colombo, I. Nova, E. Tronconi, A comparative study of the NH<sub>3</sub>-SCR reactions over a Cu-zeolite and a Fe-zeolite catalyst, *Catal. Today* 151 (2010) 223–230.
- [25] L. Olsson, K. Wijayanti, K. Leistner, A. Kumar, S.Y. Joshi, K. Kamasamudram, N.W. Currier, A. Yezersets, A kinetic model for sulfur poisoning and regeneration of Cu/SSZ-13 used for NH<sub>3</sub>-SCR, *Appl. Catal. B* 183 (2016) 394–406.
- [26] K. Supriyanto, A. Wijayanti, S. Kumar, K. Joshi, N.W. Kamasamudram, A. Currier, L. Yezersets, Olsson, Global kinetic modeling of hydrothermal aging of NH<sub>3</sub>-SCR over Cu-zeolites, *Appl. Catal. B* 163 (2015) 382–392.
- [27] I. Colbeck, B. Atkinson, Y. Johar, The morphology and optical properties of soot produced by different fuels, *J. Aerosol Sci.* 28 (1997) 715–723.
- [28] D. Uy, M.A. Ford, D.T. Jayne, A.E. O'Neill, L.P. Haack, J. Hangas, M.J. Jagner, A. Sammut, A.K. Gangopadhyay, Characterization of gasoline soot and comparison to diesel soot: morphology, chemistry, and wear, *Tribol. Int.* 80 (2014) 198–209.
- [29] C.K. Gaddam, R.L. Vander Wal, Physical and chemical characterization of SIDI engine particulates, *Combust. Flame* 160 (2013) 2517–2528.
- [30] I.C. Jaramillo, C.K. Gaddam, R.L. Vander Wal, C.-H. Huang, J.D. Levithal, J.S. Lighty, Soot oxidation kinetics under pressurized conditions, *Combust. Flame* 161 (2014) 2951–2965.
- [31] Y. Liu, C. Song, G. Lv, X. Cao, L. Wang, Y. Qiao, X. Yang, Surface functional groups and sp<sub>3</sub>/sp<sub>2</sub> hybridization ratios of in-cylinder soot from a diesel engine fueled with n-heptane and n-heptane/toluene, *Fuel* 179 (2016) 108–113.
- [32] R.L. Vander Wal, V.M. Bryg, M.D. Hays, Fingerprinting soot (towards source identification): physical structure and chemical composition, *J. Aerosol Sci.* 41 (2010) 108–117.
- [33] R. Prasad, V.R. Bella, A review on diesel soot emission, its effect and control, *Bull. Chem. React. Eng. Catal.* 5 (2010) 69–86.
- [34] D.B. Kittelson, Engines and nanoparticles: a review, *J. Aerosol Sci.* 29 (1998) 575–588.
- [35] P. Gilot, F. Marcucilli, G. Prado, Porous media and the use of thermobalances: the kinetics of combustion processes, K.G. Nickel Corrosion of Advanced Ceramics, NATO Science Series E, p. 329–339.
- [36] H. Burtscher, Physical characterization of particulate emissions from diesel engines: a review, *J. Aerosol Sci.* 36 (2005) 896–932.
- [37] M. Matti Maricq, Chemical characterization of particulate emissions from diesel engines: a review, *J. Aerosol Sci.* 38 (2007) 1079–1118.
- [38] G. Kastrinaki, S. Lorentzou, A.G. Konstandopoulos, Soot oxidation kinetics of different Ceria nanoparticle catalysts, *Emiss. Control Sci. Technol.* 1 (2015) 247–253.
- [39] A.G. Konstandopoulos, M. Kostoglou, S. Lorentzou, C. Pagkoura, E. Papaioannou, K. Ohno, K. Ogyu, T. Oya, Soot Oxidation Kinetics in Diesel Particulate Filters, SAE International, 2007.
- [40] G.R. Gavals, A random capillary model with application to char gasification at chemically controlled rates, *AIChE J.* 26 (1980) 577–585.
- [41] S.K. Bhatia, D.D. Perlmutter, A random pore model for fluid-solid reactions: I. Isothermal, kinetic control, *AIChE J.* 26 (1980) 379–386.
- [42] S.K. Bhatia, D.D. Perlmutter, A random pore model for fluid-solid reactions: II. Diffusion and transport effects, *AIChE J.* 27 (1981) 247–254.
- [43] F. Kapteijn, J.A. Moulijn, J.L. Figueiredo, J.A. Moulijn (Eds.), *Carbon and Coal Gasification*, Martinus Nijhoff Publishers, 1986, pp. 291–360.
- [44] V.P. Zhdanov, P.-A. Carlsson, B. Kasemo, Kinetics of oxidation of nm-sized soot spherules, *Chem. Phys. Lett.* 454 (2008) 341–344.
- [45] B.R. Stammore, J.F. Brilhac, P. Gilot, The oxidation of soot: a review of experiments, mechanisms and models, *Carbon* 39 (2001) 2247–2268.
- [46] J.P.A. Neeft, T.X. Nijhuis, E. Smakman, M. Makkee, J.A. Moulijn, Kinetics of the oxidation of diesel soot, *Fuel* 76 (1997) 1129–1136.
- [47] O. Mihai, S. Tamm, M. Stenfeldt, C. Wang-Hansen, L. Olsson, Evaluation of an integrated selective catalytic reduction-coated particulate filter, *Ind. Eng. Chem. Res.* 54 (2015) 11779–11791.
- [48] W. Tang, D. Youngren, M. SantaMaria, S. Kumar, On-engine investigation of SCR on filters (SCRoF) for HDD passive applications, *SAE Int. J. Engines* 6 (2013) 862–872.
- [49] O. Mihai, S. Tamm, M. Stenfeldt, L. Olsson, The effect of soot on ammonium nitrate species and NO<sub>x</sub> selective catalytic reduction over Cu-zeolite catalyst-coated particulate filter, *Philos. Trans. Math. Phys. Eng. Sci.* 374 (2016) 20150086–20150086.
- [50] E. Tronconi, I. Nova, F. Marchetti, G. Koltsakis, D. Karamitros, B. Maletić, N. Markert, D. Chatterjee, M. Hehle, Interaction of NO<sub>x</sub> reduction and soot oxidation in a DPF with Cu-Zeolite SCR coating, *Emiss. Control Sci. Technol.* 1 (2015) 134–151.
- [51] J. Tan, C. Solbrig, S.J. Schmieg, The Development of Advanced 2-Way SCR/DPF Systems to Meet Future Heavy-Duty Diesel Emissions, SAE 2011 World Congress & Exhibition.
- [52] T. Ballinger, J. Cox, M. Konduru, D. De, W. Manning, P. Andersen, Evaluation of SCR catalyst technology on diesel particulate filters, *SAE Int. J. Fuels Lubr.* 2 (2009) 369–374.
- [53] S.-Y. Park, K. Narayanaswamy, S.J. Schmieg, C.J. Rutland, A model development for evaluating Soot-NO<sub>x</sub> interactions in a blended 2-way diesel particulate filter/selective catalytic reduction, *Ind. Eng. Chem. Res.* 51 (2012) 15582–15592.
- [54] A.G. Konstandopoulos, M. Kostoglou, S. Lorentzou, N. Vlachos, Aspects of multifunctional diesel particulate filters and their efficient simulation, *Catal. Today* 188 (2012) 2–13.
- [55] F. Schrade, M. Brammer, J. Schaeffner, K. Langeheinecke, L. Kraemer, Physico-Chemical Modeling of an Integrated SCR on DPF (SCR/DPF) System, *SAE Int. J. Engines* 5 (2012) 958–974.
- [56] M. Colombo, G. Koltsakis, I. Koutoufaris, A Modeling Study of Soot and De-NO<sub>x</sub> Reaction Phenomena in SCR Systems, SAE Technical Paper, (2011), pp. 1–14.
- [57] T.C. Watling, M.R. Ravenscroft, G. Avery, Development, validation and application of a model for an SCR catalyst coated diesel particulate filter, *Catal. Today* 188 (2012) 32–41.
- [58] F. Marchetti, I. Nova, E. Tronconi, Experimental study of the interaction between soot combustion and NH<sub>3</sub>-SCR reactivity over a Cu-Zeolite SDPF catalyst, *Catal. Today* 267 (2016) 110–118.
- [59] O. Mihai, M. Stenfeldt, L. Olsson, The effect of changing the gas composition on soot oxidation over DPF and SCR-coated filters, *Catal. Today* 306 (2018) 243–250.
- [60] K. Wijayanti, S. Andonova, A. Kumar, J. Li, K. Kamasamudram, N.W. Currier, A. Yezersets, L. Olsson, Impact of sulfur oxide on NH<sub>3</sub>-SCR over Cu-SAPO-34, *Appl. Catal. B* 166 (2015) 568–579.
- [61] Avl, AVL BOOST Aftertreatment Manual, 2013.
- [62] T. Ahn, W.V. Pinczewski, D.L. Trimm, Transient performance of catalytic combustors for gas turbine applications, *Chem. Eng. Sci.* 41 (1986) 55–64.
- [63] N. Wakao, J.M. Smith, Diffusion in catalyst pellets, *Chem. Eng. Sci.* 17 (1962) 825–834.
- [64] P.S. Metkar, V. Balakotaiah, M.P. Harold, Experimental study of mass transfer limitations in Fe- and Cu-zeolite-based NH<sub>3</sub>-SCR monolithic catalysts, *Chem. Eng. Sci.* 66 (2011) 5192–5203.
- [65] B. Stanmore, J.-F. Brilhac, P. Gilot, P. Gilot, The Ignition and Combustion of Cerium Doped Diesel Soot, International Congress & Exposition.
- [66] M. Kalogirou, Z. Samaras, Soot oxidation kinetics from TG experiments, *J. Therm. Anal. Calorim.* 99 (2010) 1005–1010.
- [67] X. Auveray, W.P. Partridge, J.-S. Choi, J.A. Pihl, A. Yezersets, K. Kamasamudram, N.W. Currier, L. Olsson, Local ammonia storage and ammonia inhibition in a monolithic copper-beta zeolite SCR catalyst, *Appl. Catal. B* 126 (2012) 144–152.
- [68] F. Gao, E.D. Walter, E.M. Karp, J. Luo, R.G. Tonkyn, J.H. Kwak, J. Szanyi, C.H.F. Peden, Structure activity relationships in NH<sub>3</sub>-SCR over Cu-SSZ-13 as probed by reaction kinetics and EPR studies, *J. Catal.* 300 (2013) 20–29.
- [69] K. Leistner, K. Xie, A. Kumar, K. Kamasamudram, L. Olsson, Ammonia desorption peaks can be assigned to different copper sites in Cu/SSZ-13, *Catal. Lett.* 147 (2017) 1882–1890.
- [70] F. Göltl, R.E. Bulo, J. Hafner, P. Sautet, What makes copper-exchanged SSZ-13 zeolite efficient at cleaning car exhaust gases? *J. Phys. Chem. Lett.* 4 (2013) 2244–2249.
- [71] J.H. Kwak, H. Zhu, J.H. Lee, C.H.F. Peden, J. Szanyi, Two different cationic positions in Cu-SSZ-13? *Chem. Commun.* 48 (2012) 4758–4760.
- [72] B.C. Smith, Fundamentals of Fourier Transform Infrared Spectroscopy, CRC Press, 2011.
- [73] G. Socrates, Infrared and Raman Characteristic Group Frequencies: Tables and Charts, Wiley, 2001.
- [74] C.D. Craver, The Coblenz Society Desk Book of Infrared Spectra, (1977).
- [75] P.J. Linstrom, W.G. Mallard, NIST Chemistry WebBook, NIST Standard Reference Database Number 69, National Institute of Standards and Technology, Gaithersburg, MD, 20899.
- [76] Chemical and catalytic properties of elemental carbon, in: G.T. Wolff, R.L. Klimisch (Eds.), *Particulate Carbon - Atmospheric Life Cycle*, Springer, 1982, pp. 159–182.
- [77] N.B. Colthup, L.H. Daly, S.E. Wiberley, Chapter 11 - Amines, C=N, and N=O Compounds, Introduction to Infrared and Raman Spectroscopy, third edition, Academic Press, 1990, pp. 339–354.
- [78] A.R. Chughtai, M.M.O. Atteya, J. Kim, B.K. Konowalchuk, D.M. Smith, Adsorption and adsorbate interaction at soot particle surfaces, *Carbon* 36 (1998) 1573–1589.
- [79] A.H. Muenter, B.G. Koehler, Adsorption of Ammonia on soot at low temperatures, *J. Phys. Chem. A* 104 (2000) 8527–8534.
- [80] R.L. Vander Wal, V.M. Bryg, M.D. Hays, XPS analysis of combustion aerosols for chemical composition, surface chemistry, and carbon chemical state, *Anal. Chem.* 83 (2011) 1924–1930.
- [81] M.E. Schuster, M. Hävecker, R. Arrigo, R. Blume, M. Knauer, N.P. Ivleva, D.S. Su, R. Niessner, R. Schlügl, Surface sensitive study to determine the reactivity of soot with the focus on the European emission standards IV and VI, *J. Phys. Chem. A* 115 (2011) 2568–2580.
- [82] D.J. Growney, O.O. Mykhaylyk, L. Middlemiss, L.A. Fielding, M.J. Derry, N. Aragrag, G.D. Lamb, S.P. Armes, Is carbon black a suitable model colloidal substrate for diesel soot? *Langmuir* 31 (2015) 10358–10369.
- [83] S. Kundu, Y. Wang, W. Xia, M. Muhler, Thermal stability and reducibility of oxygen-containing functional groups on multiwalled carbon nanotube surfaces: a quantitative high-resolution XPS and TPD/TPR study, *J. Phys. Chem. C* 112 (2008) 16869–16878.
- [84] H. Tillborg, A. Nilsson, B. Hernnäs, N. Mårtensson, R.E. Palmer, X-ray and UV photoemission studies of mono-, bi- and multilayers of physisorbed molecules: O<sub>2</sub> and N<sub>2</sub> on graphite, *Surf. Sci.* 295 (1993) 1–12.

- [85] T.I.T. Okpalugo, P. Papakonstantinou, H. Murphy, J. McLaughlin, N.M.D. Brown, High resolution XPS characterization of chemical functionalised MWCNTs and SWCNTs, *Carbon* 43 (2005) 153–161.
- [86] D.H. Wang, Y. Hu, J.J. Zhao, L.L. Zeng, X.M. Tao, W. Chen, Holey reduced graphene oxide nanosheets for high performance room temperature gas sensing, *J. Mater. Chem. A* 2 (2014) 17415–17420.
- [87] K. Otto, M.H. Sieg, M. Zinbo, L. Bartosiewicz, The oxidation of soot deposits from diesel engines, *Automotive Engineering Congress and Exposition*, SAE International, 1980.
- [88] I.W. Smith, The intrinsic reactivity of carbons to oxygen, *Fuel* 57 (1978) 409–414.
- [89] H. Jung, D.B. Kittelson, M.R. Zachariah, Kinetics and visualization of soot oxidation using transmission electron microscopy, *Combust. Flame* 136 (2004) 445–456.
- [90] C.J. Tighe, M.V. Twigg, A.N. Hayhurst, J.S. Dennis, The kinetics of oxidation of Diesel soots and a carbon black (Printex U) by O<sub>2</sub> with reference to changes in both size and internal structure of the spherules during burnout, *Carbon* 107 (2016) 20–35.
- [91] K. Leistner, A. Nicolle, D. Berthout, Pd. Costa, Kinetic modelling of the oxidation of a wide range of carbon materials, *Combust. Flame* 159 (2012) 64–76.
- [92] K. Hashimoto, P.L. Silveston, Gasification: Part I. Isothermal, kinetic control model for a solid with a pore size distribution, *AIChE J.* 19 (1973) 259–268.
- [93] A. Yezerets, N.W. Currier, H. Eadler, A. Suresh, S. Popuri, Quantitative flow-reactor study of diesel soot oxidation process, *SAE 2002-01-1684* (2002).
- [94] T. Ishiguro, N. Suzuki, Y. Fujitani, H. Morimoto, Microstructural changes of diesel soot during oxidation, *Combust. Flame* 85 (1991) 1–6.
- [95] M.V. Twigg, Progress and future challenges in controlling automotive exhaust gas emissions, *Appl. Catal. B* 70 (2007) 2–15.
- [96] C.J. Tighe, M.V. Twigg, A.N. Hayhurst, J.S. Dennis, The kinetics of oxidation of Diesel soots by NO<sub>2</sub>, *Combust. Flame* 159 (2012) 77–90.
- [97] C.M. Long, M.A. Nascarella, P.A. Valberg, Carbon black vs. black carbon and other airborne materials containing elemental carbon: physical and chemical distinctions, *Environ. Pollut.* 181 (2013) 271–286.
- [98] R.C. Everson, H.W.J.P. Neomagus, H. Kasaini, D. Njapha, Reaction kinetics of pulverized coal-char derived from inertinite-rich coal discards: Gasification with carbon dioxide and steam, *Fuel* 85 (2006) 1076–1082.
- [99] K.Y. Lisandy, G.-M. Kim, J.-H. Kim, G.-B. Kim, C.-H. Jeon, Enhanced accuracy of the reaction rate prediction model for carbonaceous solid fuel combustion, *Energy Fuels* 31 (2017) 5135–5144.
- [100] T. Holland, T.H. Fletcher, Comprehensive model of single particle pulverized coal combustion extended to oxy-coal conditions, *Energy Fuels* 31 (2017) 2722–2739.
- [101] M. Frenklach, H. Wang, Detailed modeling of soot particle nucleation and growth, *Symp. (Int.) Combust.* 23 (1991) 1559–1566.
- [102] M. Celnik, A. Raj, R. West, R. Patterson, M. Kraft, Aromatic site description of soot particles, *Combust. Flame* 155 (2008) 161–180.
- [103] A. Raj, G.R. da Silva, S.H. Chung, Reaction mechanism for the free-edge oxidation of soot by O<sub>2</sub>, *Combust. Flame* 159 (2012) 3423–3436.
- [104] M. Frenklach, Z. Liu, R.I. Singh, G.R. Galimova, V.N. Azyazov, A.M. Mebel, Detailed, sterically-resolved modeling of soot oxidation: role of O atoms, interplay with particle nanostructure, and emergence of inner particle burning, *Combust. Flame* 188 (2018) 284–306.
- [105] R.F. Strickland-Constable, The interaction of oxygen and carbon filaments at high temperatures, *Trans. Faraday Soc.* 40 (1944) 333–343.
- [106] J. Nagle, R.F. Strickland-constable, Oxidation of carbon between 1000–2000°C, *Proceedings of the Fifth Conference on Carbon* (1962) 154–164.
- [107] J.R. Walls, R.F. Strickland-Constable, Oxidation of carbon between 1000–2400°C, *Carbon* 1 (1964) 333–338.
- [108] Y. Gao, A. Duan, S. Liu, X. Wu, W. Liu, M. Li, S. Chen, X. Wang, D. Weng, Study of Ag/Ce<sub>x</sub>Nd<sub>1-x</sub>O<sub>2</sub> nanocubes as soot oxidation catalysts for gasoline particulate filters: Balancing catalyst activity and stability by Nd doping, *Appl. Catal. B* 203 (2017) 116–126.
- [109] O.A. Shromova, N.M. Kinnunen, T.A. Pakkanen, M. Suvanto, Promotion effect of water in catalytic fireplace soot oxidation over silver and platinum, *RSC Adv.* 7 (2017) 46051–46059.
- [110] C. Lee, Y. Jeon, S. Hata, J.-I. Park, R. Akiyoshi, H. Saito, Y. Teraoka, Y.-G. Shul, H. Einaga, Three-dimensional arrangements of perovskite-type oxide nano-fiber webs for effective soot oxidation, *Appl. Catal. B* 191 (2016) 157–164.
- [111] D.E. Edwards, D.Y. Zubarev, W.A. Lester, M. Frenklach, Pathways to Soot Oxidation: Reaction of OH with Phenanthrene Radicals, *J. Phys. Chem. A* 118 (2014) 8606–8613.